Mapping the 2021/2022 Boulder County Marshall Fire

Evaluating and Comparing Landsat8 and Landsat9 Satellites to Map Wildfire Burn Areas

Figure 1. Marshall Fire consumes residence in Boulder County, Colorado. (Jeremy Sparig, Special to The Colorado Sun, 2021) Reproduced here for educational purposes only.

Raelyn Caldwell

GEOG 596B

Capstone – Final Report

08/03/2022

Advisor: Dr. Alan Taylor

Table of Contents

Figures

Tables

Abstract: As wildfires increase in occurrence and severity across the United States, technology continually plays an important role in wildfire emergency preparation and response. Remotely sensed satellite images can be used for fire detection, active fire mapping, post-fire burn scar and burn area mapping, as well as damage assessments. The Landsat8 OLI/TIRS and Landsat9 OLI/TIRS-2 satellites orbit the Earth capturing 740 scenes a day in 11 spectral bands at 30-meter spatial resolution (USGS, n.d.-a; USGS, n.d.-b). The Landsat9 satellite, launched in September 2021, improved upon its predecessor with an increased radiometric resolution of 14-bit. This means the new Landsat9 satellite can distinguish over 16,000 shades in each wavelength of the electromagnetic spectrum. The Landsat8's 12-bit satellite can distinguish only over 4,000 shades.

The Marshall Fire started burning December 31, 2021, in Boulder County, Colorado and burned across two cities creating a burn area of over than 6,000 acres before heavy overnight snowfall extinguished the fire January 1, 2022. This paper presents a supervised pixel-based image analysis classification process performed on two sets of satellite captured pre-fire imagery and post-fire imagery to map and quantify burn area within the Marshall Fire perimeter. Landsat8 OLI/TIRS and Landsat9 OLI/TIRS-2 imagery was acquired for the study areas. The image classification process performed in ArcGIS Pro included preprocessing the vector and raster data, creating training samples and classification, and an accuracy assessment. Classifying the images into seven classes (water, developed, barren, vegetation, grassland, pavement, and shadow) allowed for creating distinct classes to compare the accuracy of classification between the Landsat8 satellite and the new Landsat9 satellite. Creating difference rasters by subtracting the post-fire classified images from the pre-fire classified images resulted in a binary burned and unburned image for each of the satellites being evaluated. The replicable process resulted in successful image classification and identification and quantification of burned areas within the Marshall Fire perimeter.

Keywords: Remote Sensing, Accuracy Assessment, Wildfire Mapping, Landsat8, Landsat9, Supervised Classification, Pixel-based Classification

1. Introduction

Climate change and human activities have been increasing the occurrence of large wildfires events across the world, and especially in the western United States. As these fires become more and more damaging, fire and emergency management agencies are turning to remote sensing to evaluate the impacts and effects of wildfires on communities and ecosystems. Technology that is continually evolving plays an increasingly important role in preventing, detecting, responding to, managing, and developing post-fire recovery plans, and remote sensing is central to this effort. Remotely sensed satellite images can be used for fire detection, active fire mapping, post-fire burn scar and burn area mapping, as well as damage assessments.

Developments improving spectral and radiometric resolutions on remote sensing satellites provides new opportunities to assess the current accuracy of burn area mapping. As part of the National Land Imaging (NLI) program, the Land Remote-Sensing Satellites (Landsat) Missions have, until recently, been comprised of eight Earth-observing satellites using remote sensors to image our planet (NASA Landsat Science, n.d.). The Landsat9 mission was recently launched on September 27th, 2021, marking the next evolution of the Landsat program. Landsat9 improvements include higher radiometric resolution across the visible spectrum, to achieve greater sensitivity to brightness and color; otherwise, the design and instruments aboard Landsat9 replicate those found on Landsat8.

Water bodies and shadows in imagery can often be confused with burned areas due to their similar spectral properties, affecting the accuracy of burnt area estimates derived from

remotely sensed data (Pereira et. al., 1999). Water has low and steadily decreasing reflectance with wavelengths, particularly in the visible spectrum, with almost no reflectance in the near infrared range. This means water surfaces will appear as dark areas (low pixel values) when an image is displayed using a band combination that utilizes the red, green, blue, NIR, or SWIR bands. Shadows naturally have low pixel values and will appear as dark areas in imagery as well.

This study will evaluate the ability of remote sensing indices derived from the newly launched Landsat9 OLI-2/TIRS-2 satellite to identify and assess the burn area of a recent fire in Colorado, the Marshall Fire and compare the results to those derived from the Landsat8 OLI/TIRS satellite. It is predicted that the classification process applied to the Landsat9 imagery will result in substantially improved accuracy due to its higher radiometric resolution. The most common burn index is the Normalized Burn Ratio (NBR), which is used to detect burned areas and provide a measure of burn severity by utilizing the Near Infrared (NIR) and Shortwave Infrared (SWIR) bands. A variation of the NBR will also be used: the difference NBR (dNBR). These indices are discussed further in the methodology section.

Figure 2. Wildfire flames and smoke rise above Superior, Colorado. (Van Denburg for CPR News, 2022) Reproduced here for educational purposes only.

2. Study Area

The study area chosen for this project is the landscape within and around the Marshall Fire perimeter, the final area totaling over 6,026 acres. The Marshall Fire burned for 2 days in Boulder County, Colorado causing 35,000 people to be evacuated within and surrounding the fire perimeter (Camero, 2021). Without heavy snowfall the night of New Year's Eve, fire and emergency personnel suspect the fire could have grown much larger due to high winds and dry conditions (Andone & Maxouris, 2021). This area of Colorado, often referred to as Colorado's Front Range, experienced a humid spring causing above average amounts of grass to grow, followed by a warm and dry summer and little snow in the winter creating "…ideal weather conditions for wildfire," (Bellisle, 2022).

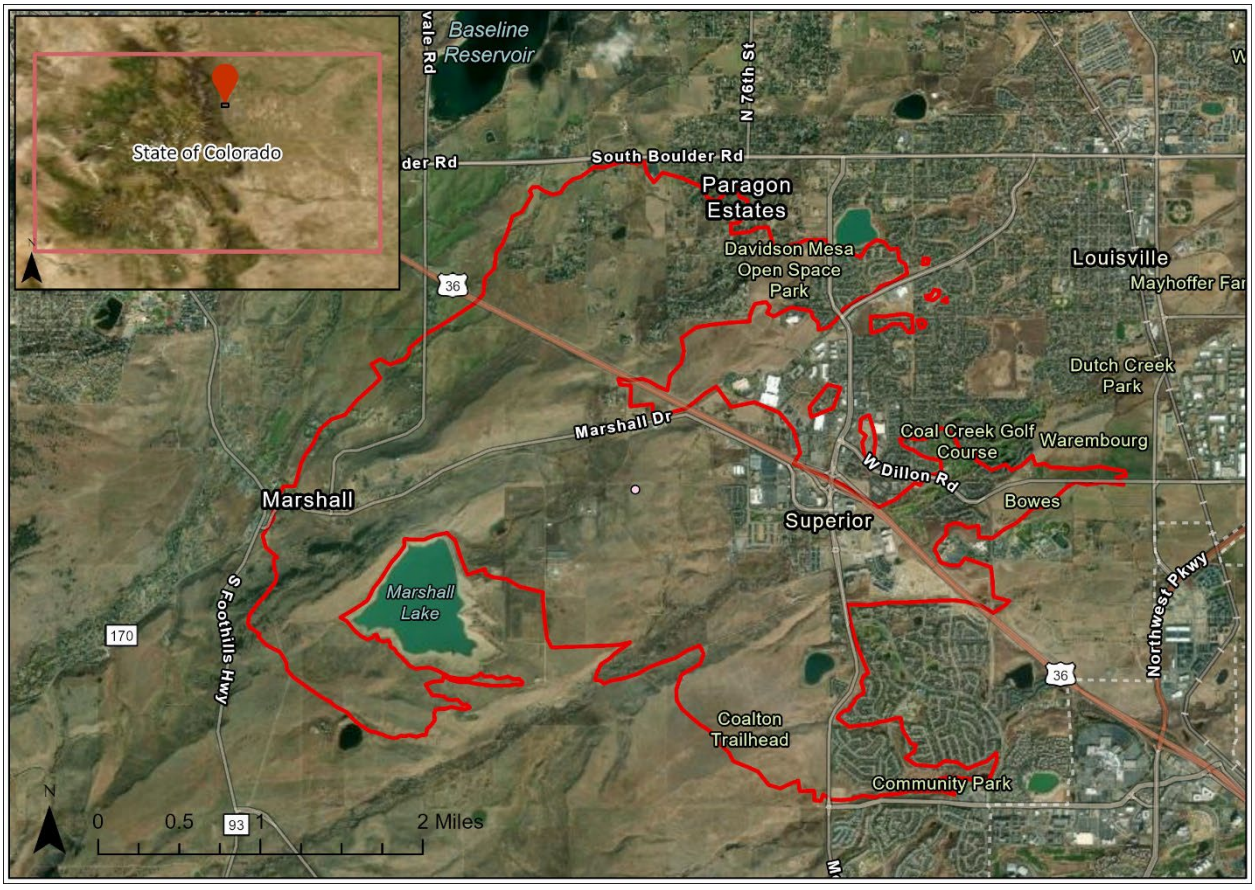

Figure 2. Study area map: Marshall Fire burn area perimeter overlayed on the Esri Imagery basemap.

3. Data & Software

ArcGIS Pro version 2.8.3 was used for preprocessing the vector and raster datasets for the project, as well as for performing the image classifications and accuracy assessment. Microsoft Excel was utilized to visualize the results of the accuracy assessment error matrices.

Vector and raster data were used in this project, as detailed in Table 1 and Table 2 below, and were acquired from public sources. The various perimeter data was extracted from government open data sites, while the satellite imagery was downloaded from the USGS EarthExplorer website. Satellite imagery was acquired for before the fire, 12/04/2021 (Landsat8) and 12/21/2021 (Landsat9), and after the fire, 04/28/2022 (Landsat8) and 04/04/2022 (Landsat9). One Landsat8 scene and Landsat9 scene per time period sufficiently covered the project area.

Format	Name	Coordinate System	Source
Shapefile	Colorado State Boundary	Colorado State Plane N, 1992 HARN	CDPHE Open Data
Shapefile	Boulder County Boundary	Colorado State Plane N, 1992 HARN	BoulderCounty Admin
Shapefile	Town of Superior Boundary	Colorado State Plane N, 1992 HARN	AlexBTOS
Shapefile	City of Louisville Boundary	Colorado State Plane N, 1992 HARN	Louisville Planning Dept.
Shapefile	Marshall Fire Perimeter	Colorado State Plane N, 1992 HARN	OpenData Boulder County

Table 1. Vector data acquired for project.

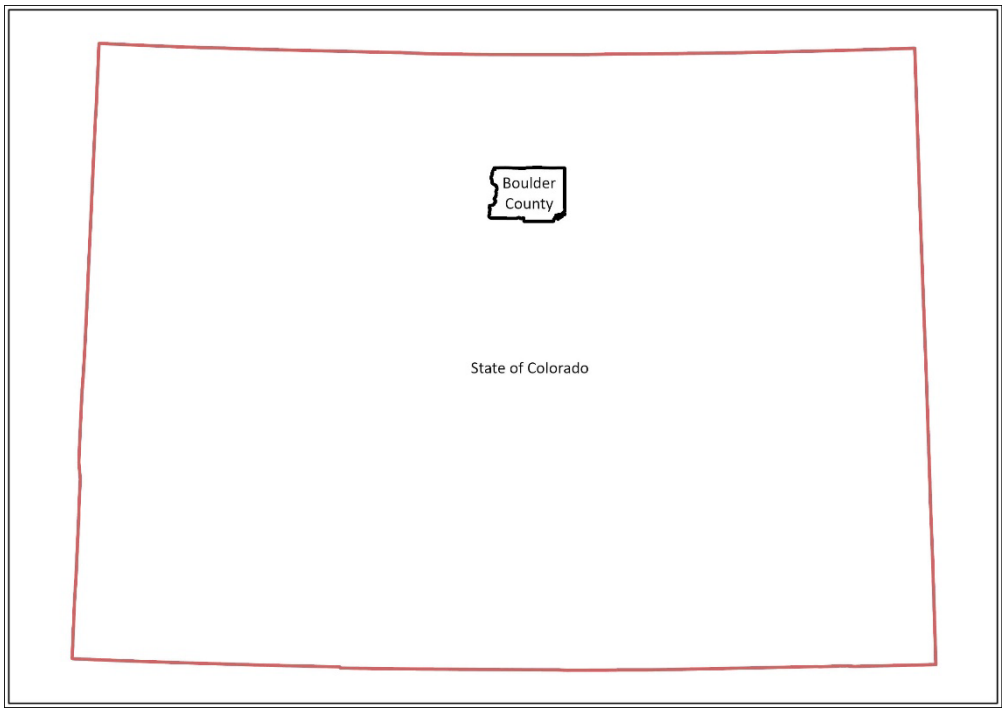

Figure 4. Colorado State boundary (red) and the Boulder County boundary (black).

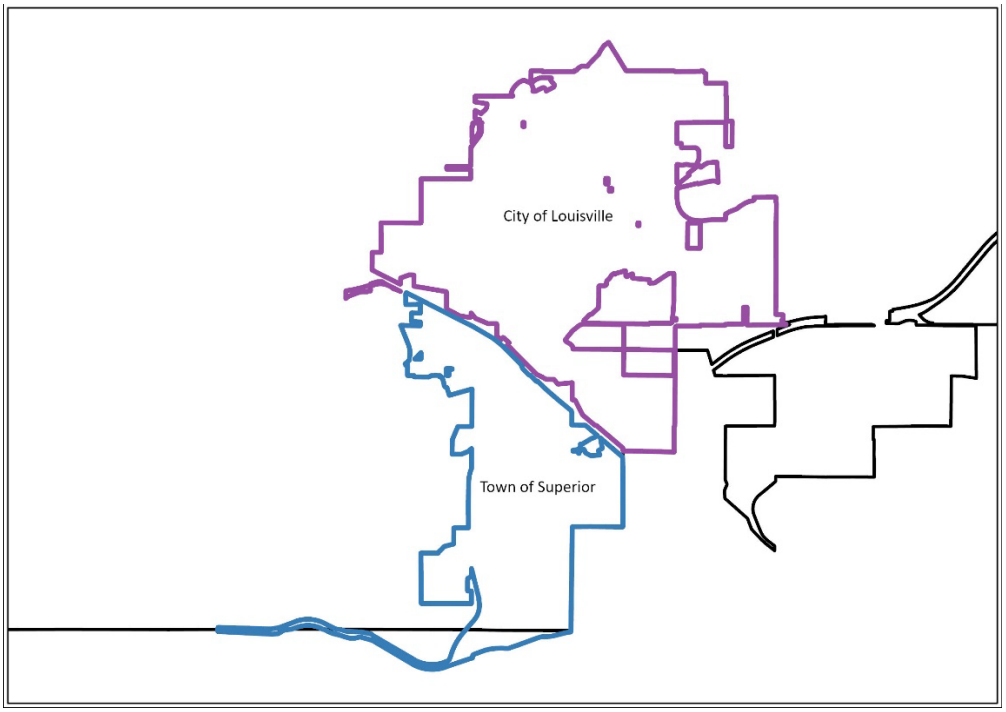

Figure 5. City of Louisville boundary (purple) and the Town of Superior boundary (blue).

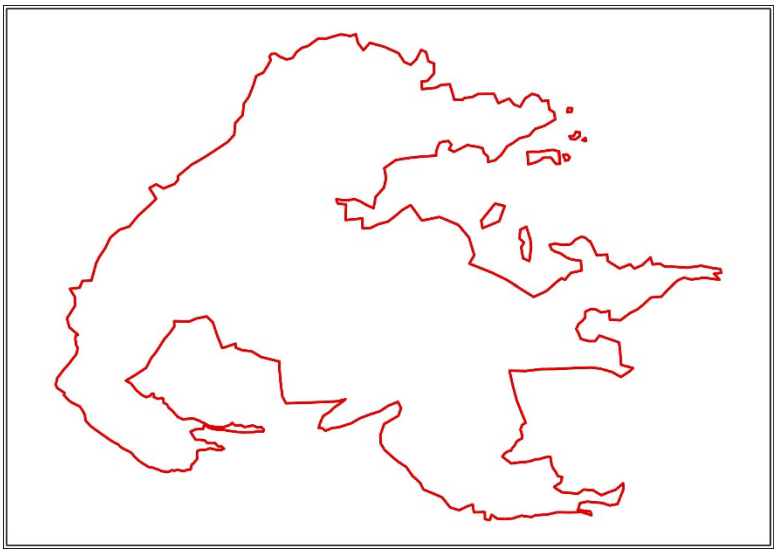

Figure 6. Marshall Fire perimeter.

Format	Name	Sensor	Date Captured	Spatial Resolution (meters)	Radiometric Resolution	Bands	Source
JPG2000	LC08_L1TP_033032_20211221_20211229_02_T1	Landsat8 OLI/TIRS	12-21-2021	30	12-bit	11	USGS Earth Explorer
JPG2000	LC08_L1TP_033032_20220428_20220503_02_T1	Landsat8 OLI/TIRS	04-28-2022	30	12-bit	11	USGS Earth Explorer
JPG2000	LC09_L1TP_034032_20211204_20220120_02_T1	Landsat9 OLI/TIRS-2	12-04-2021	30	14-bit	11	USGS Earth Explorer
JPG2000	LC09_L1TP_033032_20220404_20220405_02_T1	Landsat9 OLI/TIRS-2	04-04-2022	30	14-bit	11	USGS Earth Explorer

Table 2. Raster data acquired for project.

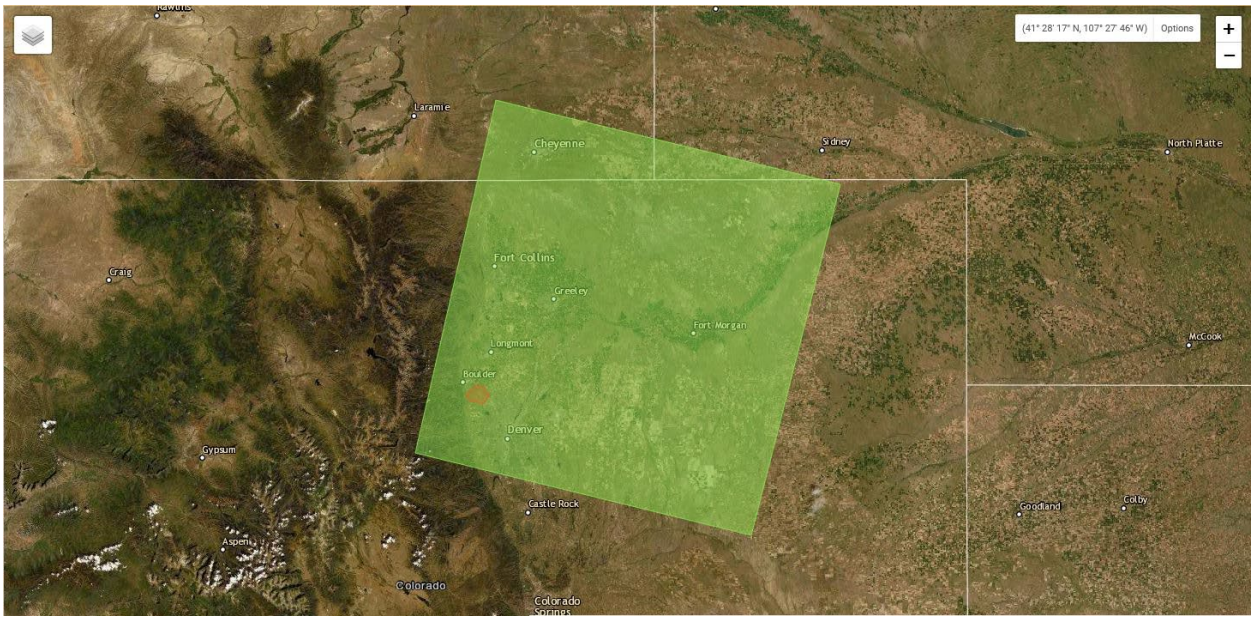

Figure 7. Example Landsat8 scene footprint. Screenshot of the USGS EarthExplorer data search results window.

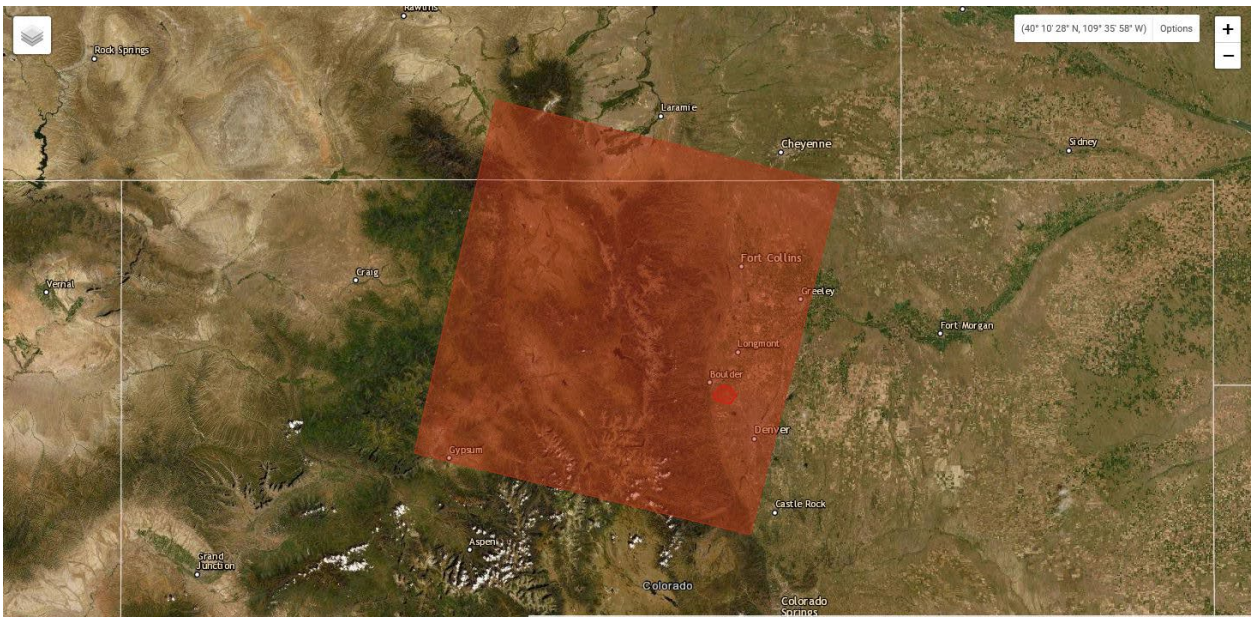

Figure 8. Example of Landsat9 scene footprints. Screenshot of the USGS EarthExplorer data search results window.

4. Detailed Workflow

Figure 9 displays a simplified project workflow from acquiring the data necessary for analysis to completing the accuracy assessment. First, the data was preprocessed to buffer the fire burn area perimeter to encompass surrounding land cover and use types to best test the accuracy of classification between the Landsat8 and Landast9 satellites. Because the vector data for the project was acquired from various Colorado government agencies, no vector data needed to be reprojected or otherwise manipulated for this project. Next, the images were preprocessed to create composite bands, be projected to the Colorado StatePlane Zone 13 projection, and clipped to the buffered fire burn area perimeter. The preprocessed images were then used to create training samples and spectral profiles, before being classified, and finally an accuracy assessment was performed.

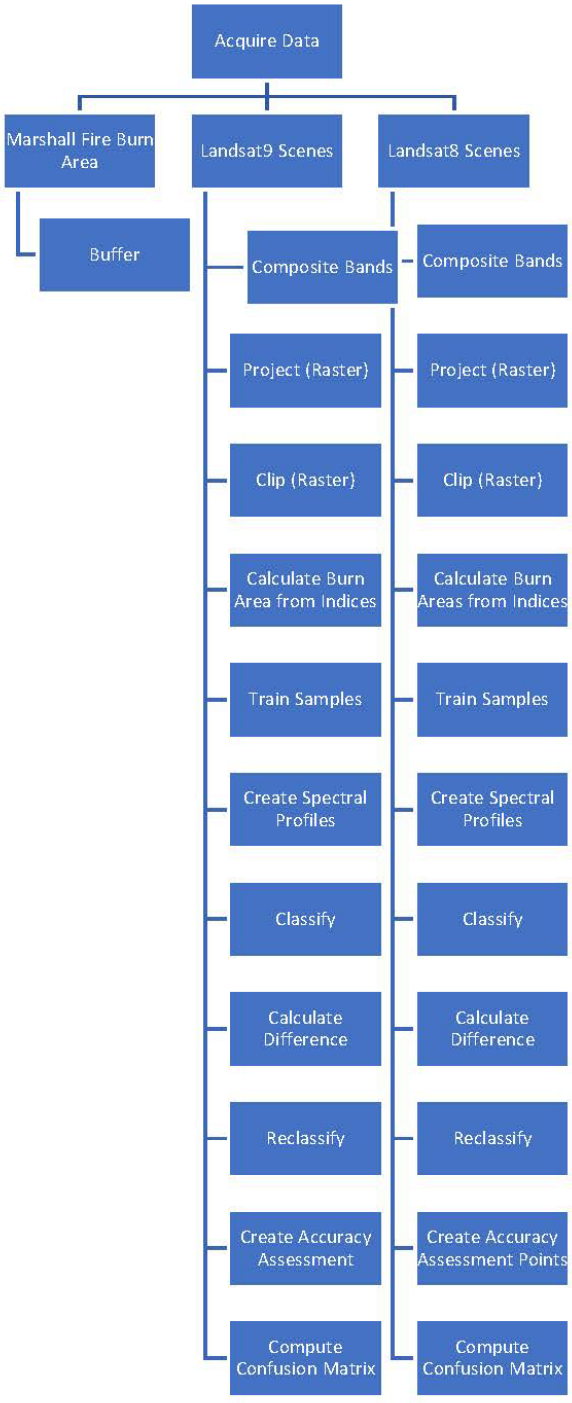

Figure 9. Project workflow.

4.1 Data Preprocessing

The only vector data that needed preprocessing was the Marshall Fire Perimeter shapefile, which was buffered to allow for additional landcover and use classes to be included in the supervised pixel-based classification. Without buffering the original shapefile, there would be very few developed, vegetation, or pavement landcover/landuse classes to include in the assessment. The Colorado StatePlane projected coordinate system was used for this project because this is the system used within Colorado, with Zone 13 encompassing Boulder County where the Marshall Fire burned (Boulder County GIS, 2022).

To prepare the Landsat8 and Landsat9 raster data for analysis, the eleven bands to be used needed to be combined to create one single image per footprint using the *Composite Bands* tool. This resulted in four images with eleven bands each, two images for each time period being studied. Next, the Landsat8 and Landsat9 imagery were projected to the Colorado StatePlane Zone 13 projected coordinate system using the *Project Raster* tool and each image was clipped, using the *Clip (Raster)* tool, to the Marshall Fire burn area buffered feature class. The clipping was performed to decrease processing time and create clean edges of the images to exclude imagery outside the project area.

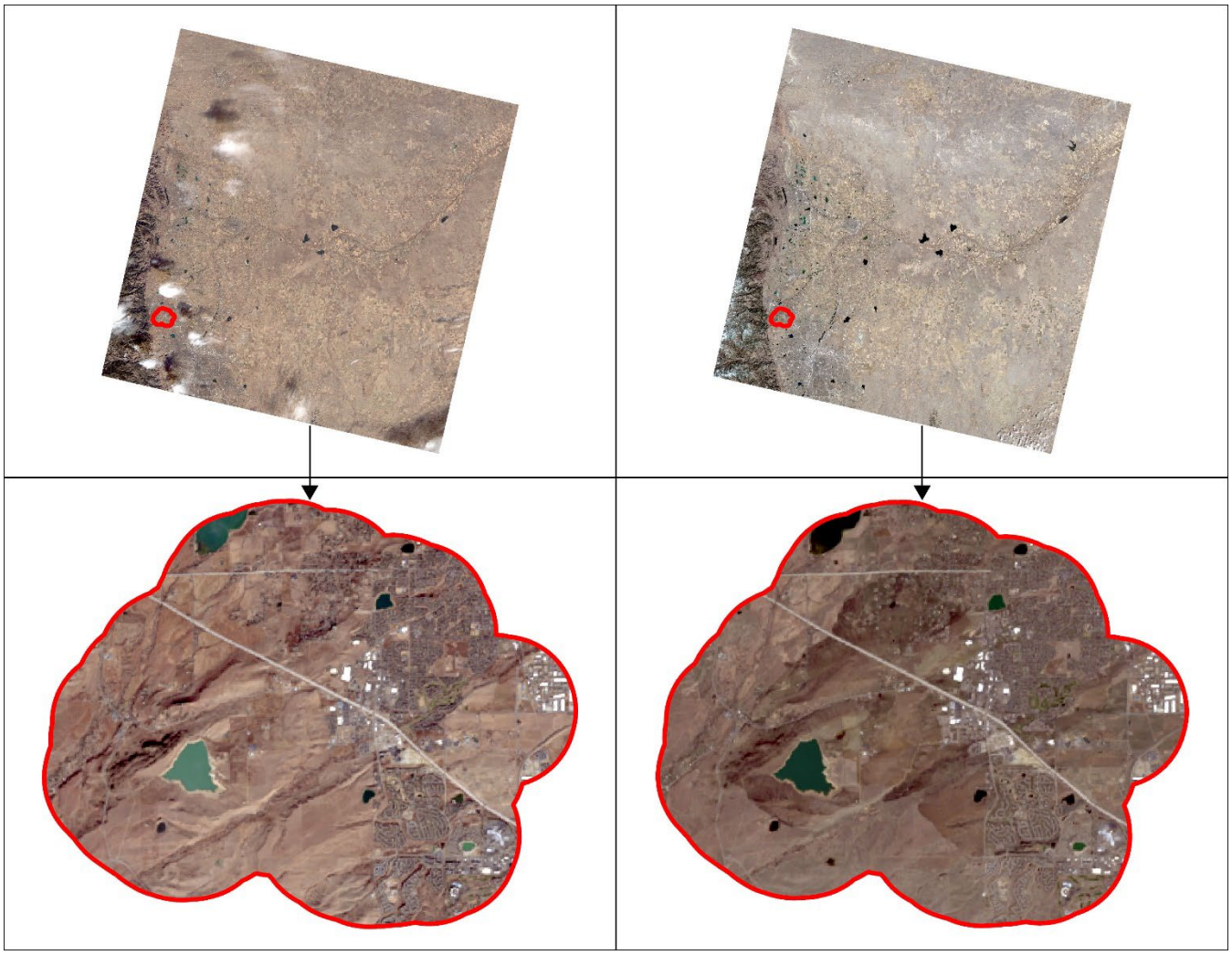

Figure 10. Results of image preprocessing. On the left, the pre-fire Landsat8 (30m) scene displayed in a Natural Color (RGB) band combination (4, 3, 2) clipped to the buffered Marshall Fire burn area perimeter. On the right, the post-fire Landsat9 (30m) scene displayed in a Natural Color (RGB) band combination (4, 3, 2) clipped to the buffered Marshall Fire burn area perimeter.

4.2 Burn Area Indices

Common indices were used to highlight the areas in the both the Landsat8 and Landsat9 pre- and post-fire images that burned as a result of the Marshall Fire. Using the Near Infrared (NIR) (Band 4) and Shortwave Infrared (SWIR) (Band 7), the Normalized Burn Ratio formula was calculated.

$$NBR = \frac{NIR-SWIR}{NIR+SWIR}$$

Figure 11. Normalized Burn Ratio formula.

The resulting raster images created from this process were then used in the Difference NBR calculation, where the post-fire NBR images are subtracted from the pre-fire NBR images. Figures 12 displays the results of this operation using a stretch color ramp, where red represents higher severity burn areas (dNBR values closer to 1) and the yellow to green portion of the color ramp represent unburned areas or areas with regrowth (dNBR values closer to -1).

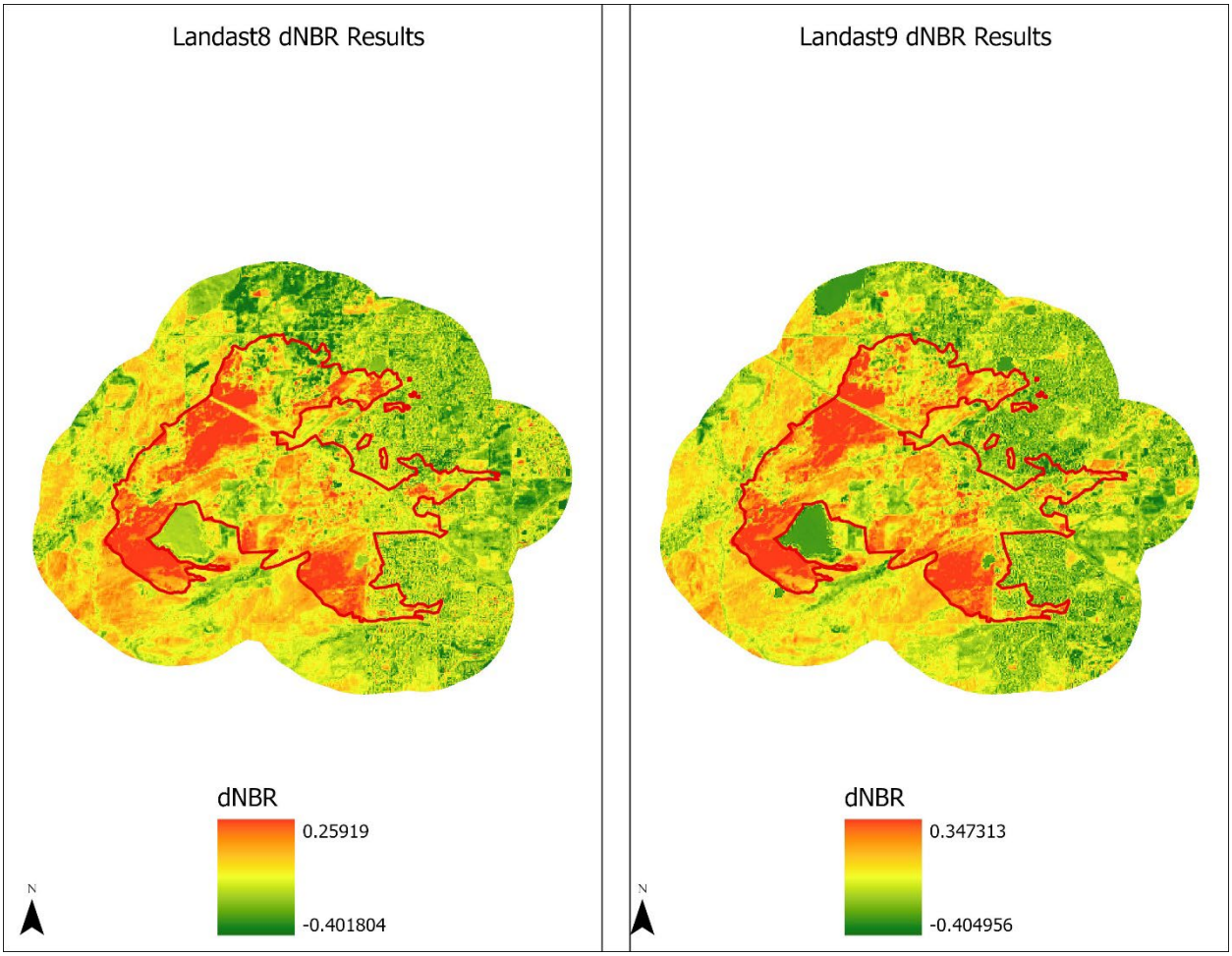

Figure 12. Results of dNBR calculations for both the Landsat8 and Landsat9 set of images, with burn areas and their severity displayed in red. Areas with yellow to green represent areas with no burn or areas of regrowth after the Marshall Fire.

4.3 Image Classification

With the vector and raster data preprocessed, the next steps were taken to classify the pre- and post-fire Landsat8 and Landsat9 imagery. All images were displayed and processed in the Natural Color band combination, RGB (4, 3, 2), as this band combination clearly visualizes the features of interest in the images. Using the set of tools under in the Image Classification tab, *Classification Tools,* the Landsat8 and Landsat 9 images were used to create training samples and classified.

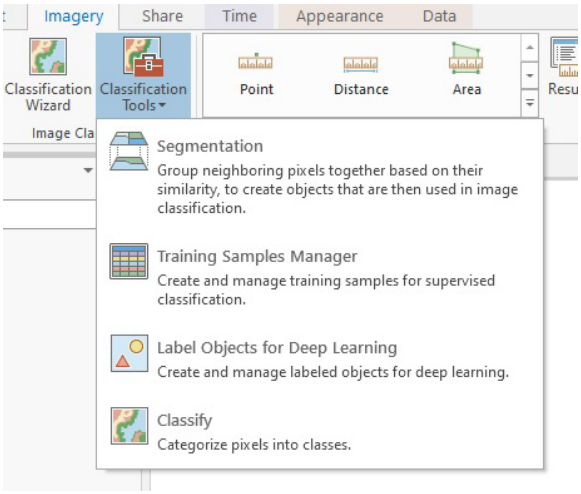

Figure 13. Screenshot of the classification tools used to classify the Landsat8 and Landsat9 images.

To create training samples, each image was used to create landcover and landuse training samples by digitizing polygons over pixels of each of the seven class types: Water, Developed, Barren, Vegetation, Grassland, Pavement, and Shadow. The vegetation class includes tree and shrub features, while the grassland class includes only grass features in the imagery. This distinction was made to capture the woody features and herbaceous features separately. Each of the four images were used to create at least 25 training samples for each class.

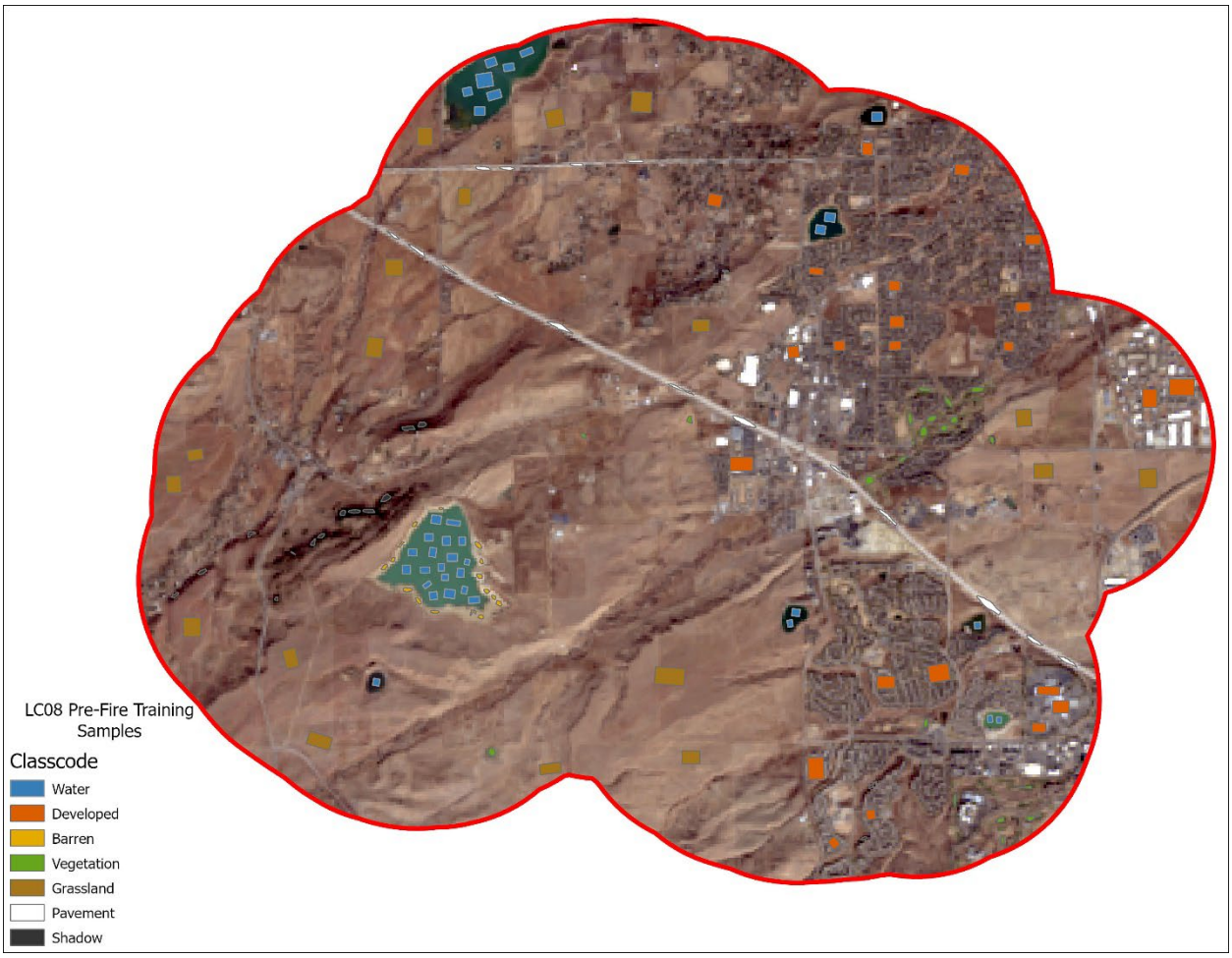

Figure 14. Example of training samples created to input into classifier. Landsat8 pre-fire image displayed in a Natural Color band combination (4, 3, 2), with training samples digitized in each of the seven classes.

These training samples were used to create spectral profiles for each class, in each of the pre- and post-fire images. These spectral profile charts allow for reviewing spectral information for each band by displaying a mean line plot of the mean values within a set of pixels for each band (Esri, n.d.). Creating these profiles can help to assist in better classifying the images by studying the pixel's spectral range to determine if training samples have been created over pixels with that may contain multiple classes or if more training samples are needed to better pick up the pixel values across the classes.

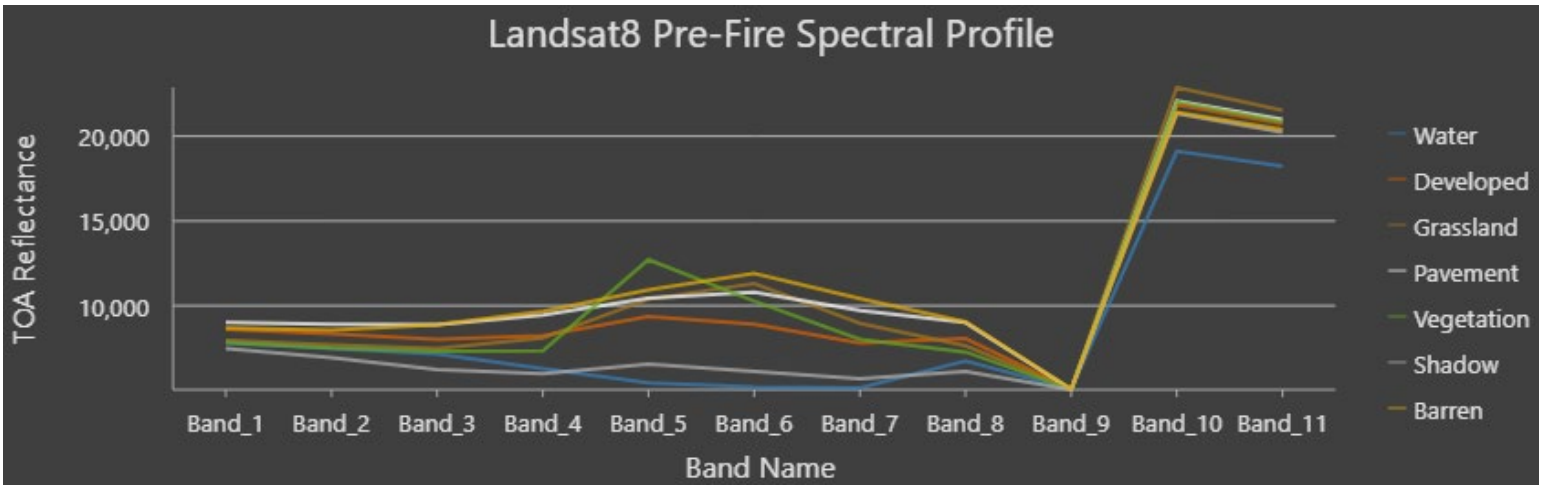

Figure 15. Spectral profile created in ArcGIS Pro for the pre-fire Landsat8 image. This profile displays the mean plot line of each of the classification classes across each of the 11 bands.

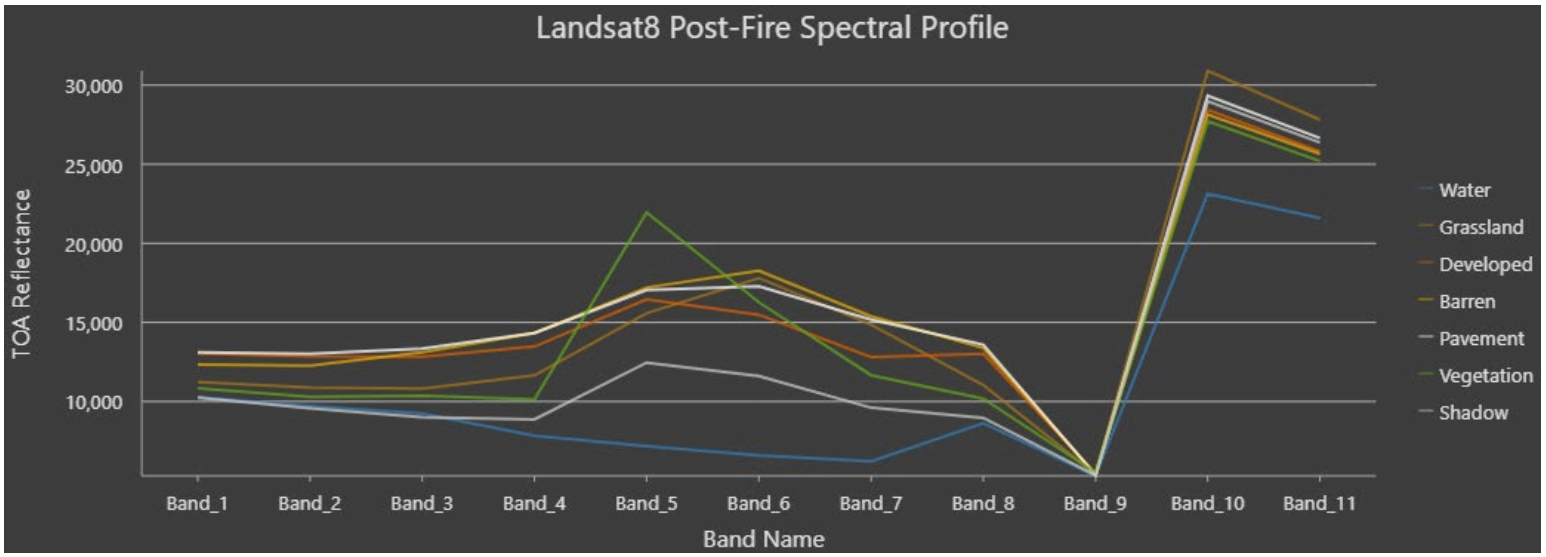

Figure 16. Spectral profile created in ArcGIS Pro for the post-fire Landsat8 image. This profile displays the mean plot line of each of the classification classes across each of the 11 bands.

Evaluating the spectral profiles for the pre- and post-fire Landsat8 imagery reveal distinct profiles between the different bands that should produce good classification results. It is expected that barren, pavement, and developed classes will have high reflectance across all wavelengths while shadow and water have lower mean values. Between the pre- and post-fire imagery, vegetation's reflectance in Band 5 (Near Infrared) is high, and even higher in the post-fire imagery, clearly indicates healthy vegetation.

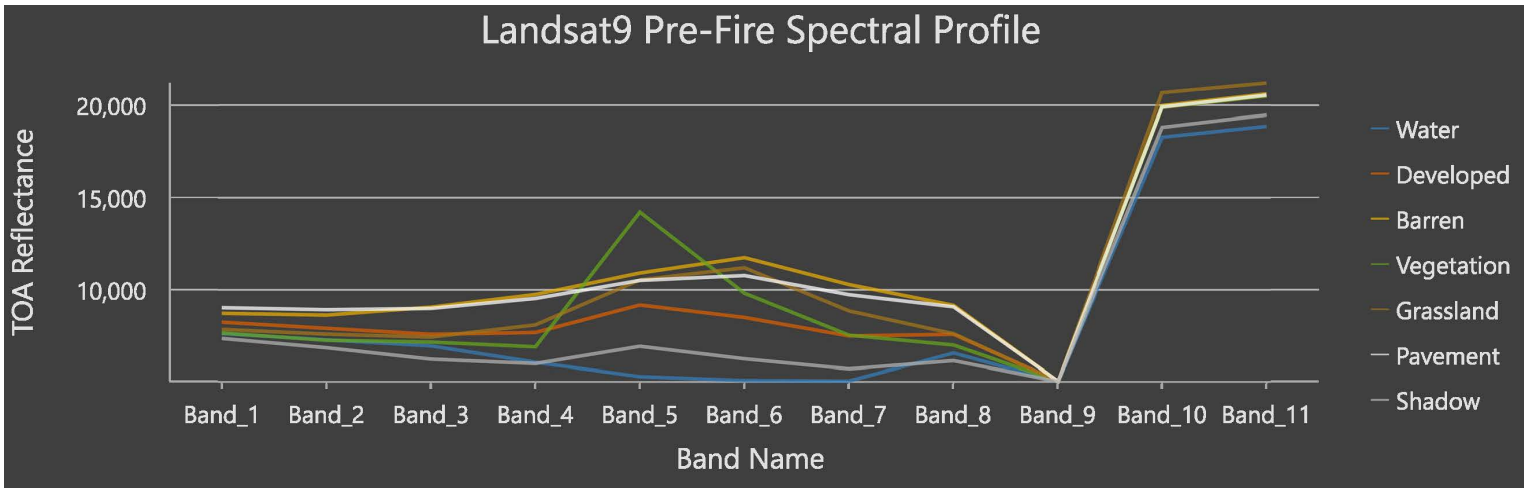

Figure 17. Spectral profile created in ArcGIS Pro for each of the pre-fire Landsat9 image. This profile displays the mean plot line of each of the classification classes across each of the 11 bands.

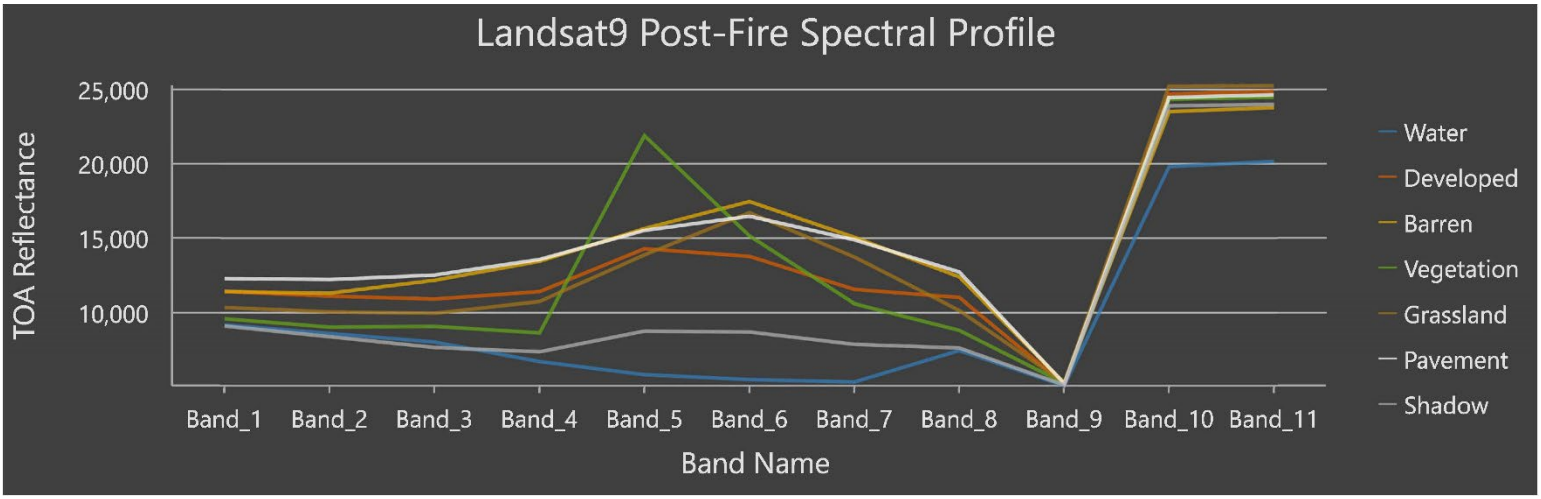

Figure 18. Spectral profile created in ArcGIS Pro for each of the post-fire Landsat9 image. This profile displays the mean plot line of each of the classification classes across each of the 11 bands.

Assessing the spectral profiles for the pre- and post-fire Landsat9 imagery also display discrete profiles across the different bands. The Landsat9 spectral profiles are similar to the Landsat8 profiles but display slight variances that are likely due to Landsat9's higher radiometric resolution, allowing the satellite to differentiate between very similar shades in each wavelength.

Being comfortable with these spectral profiles, the images were classified using the *Classify* tool from the *Classification Tools* gallery. The Maximum Likelihood classifier was used as it is well suited for testing the accuracy of classification results between Landsat8 and Landsat9 by allocating "…a pixel to the class that has the highest probability under the assumption that the reflectance values of each class have a normal (Gaussian) distribution in the band," (Woo, et al, 2021).

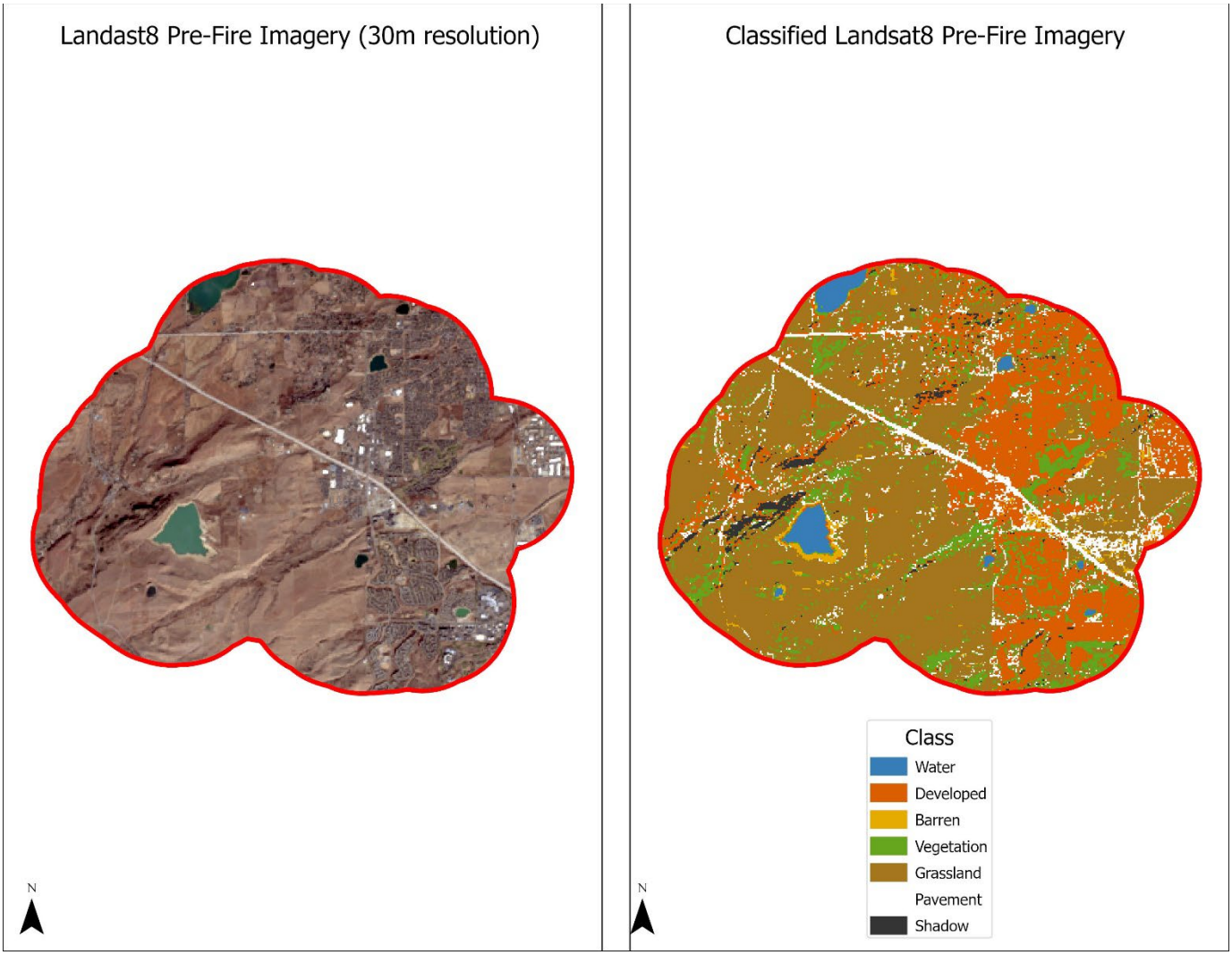

Figure 19. Results of supervised pixel-based image classification on the Landsat8 pre-fire imagery (30m). On the left, the Landsat8 image displayed in a Natural Color band combination (4, 3, 2) and on the right the classified image.

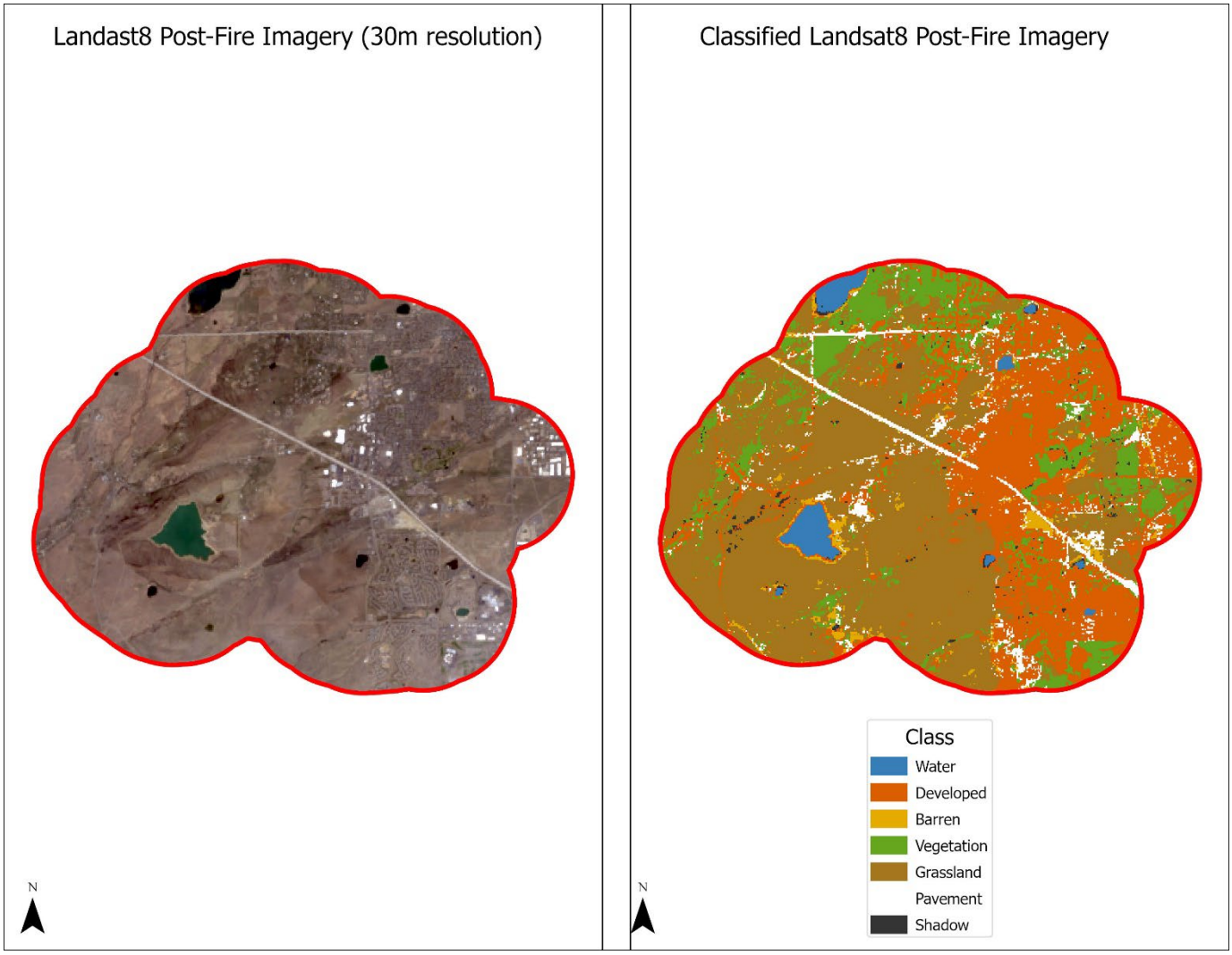

Figure 20. Results of supervised pixel-based image classification on the Landsat8 post-fire imagery (30m). On the left, the Landsat8 image displayed in a Natural Color band combination (4, 3, 2) and on the right the classified image.

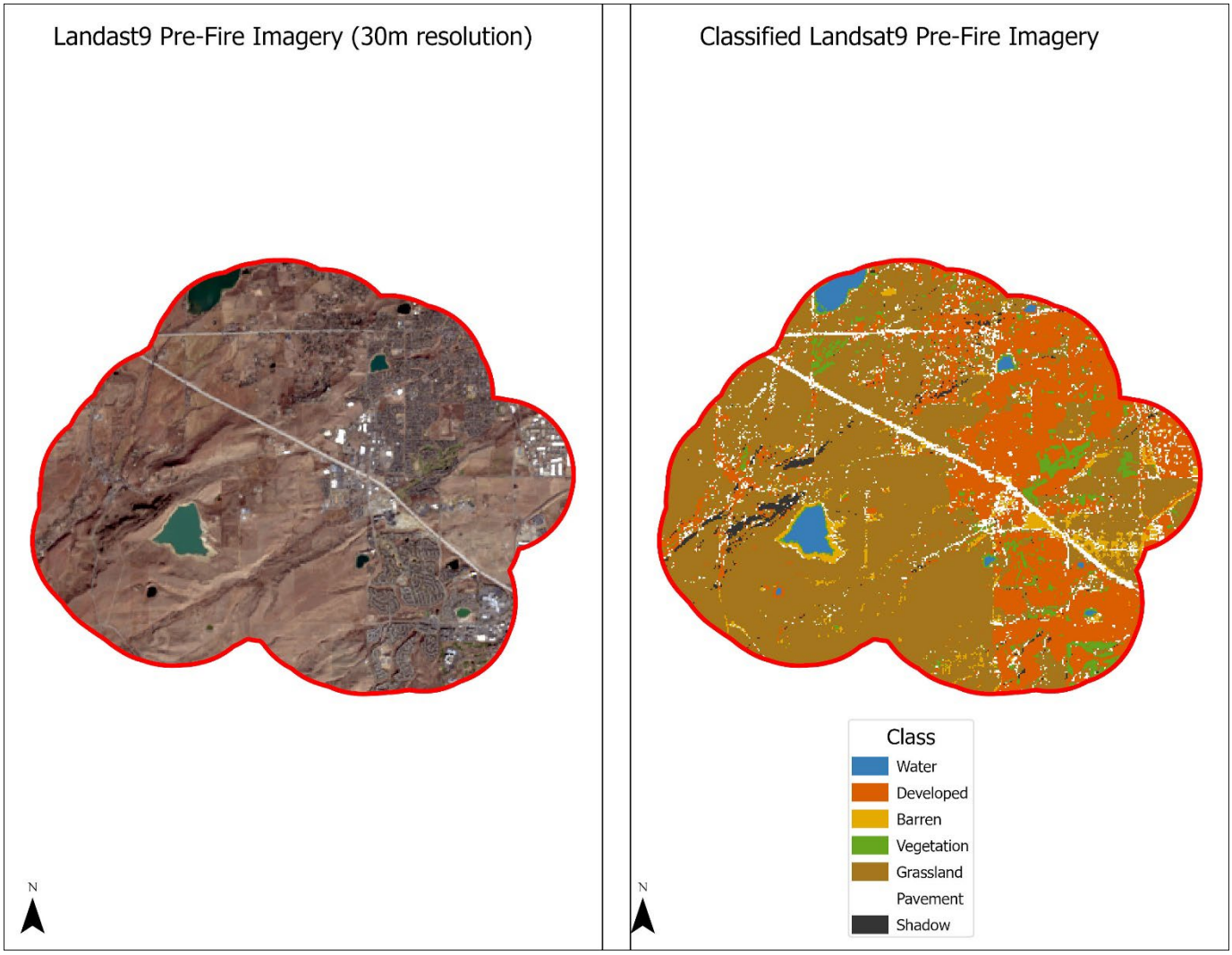

Figure 21. Results of supervised pixel-based image classification on the Landsat9 pre-fire imagery (30m). On the left, the Landsat9 image displayed in a Natural Color band combination (4, 3, 2) and on the right the classified image.

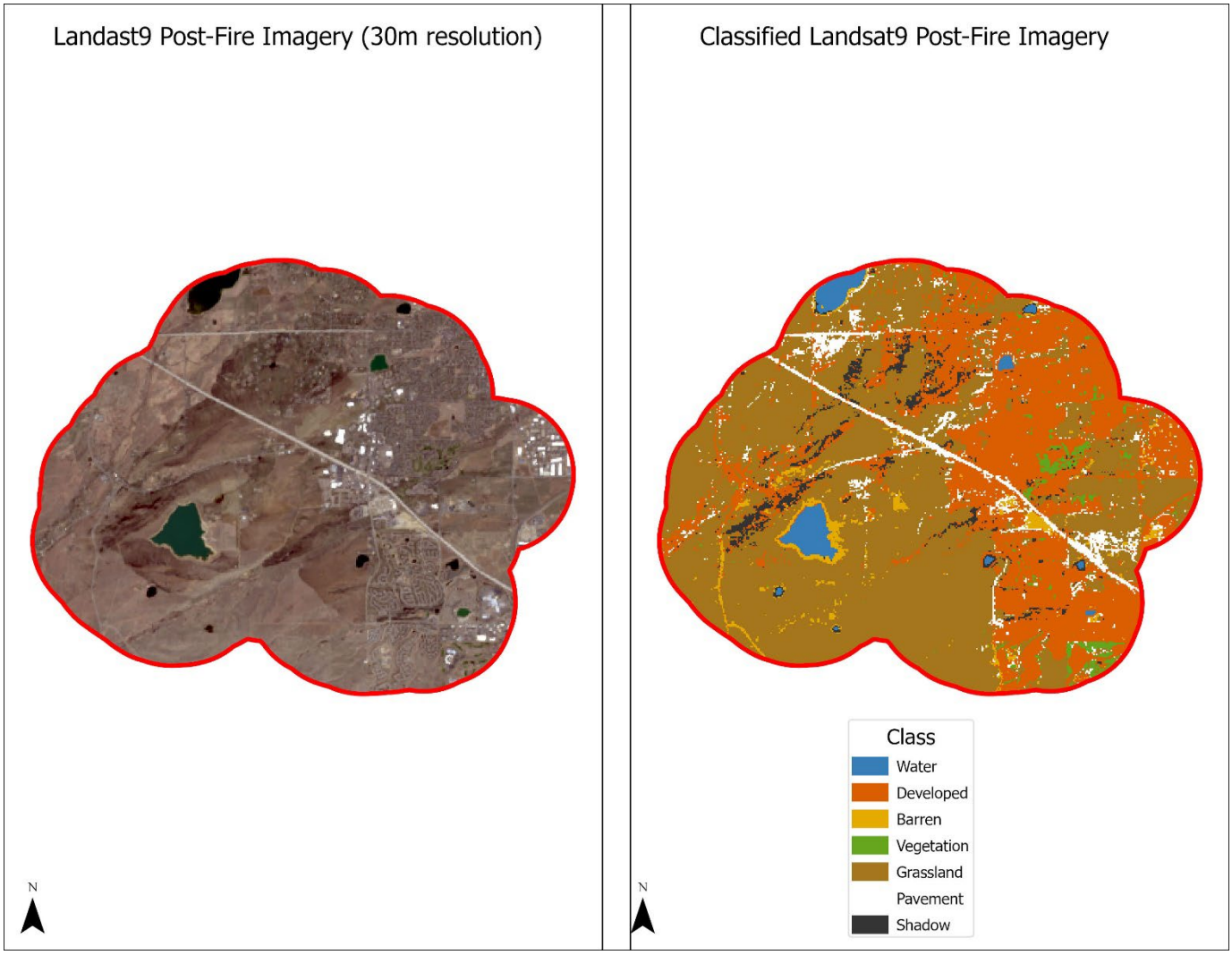

Figure 22. Results of supervised pixel-based image classification on the Landsat9 post-fire imagery (30m). On the left, the Landsat9 image displayed in a Natural Color band combination (4, 3, 2) and on the right the classified image.

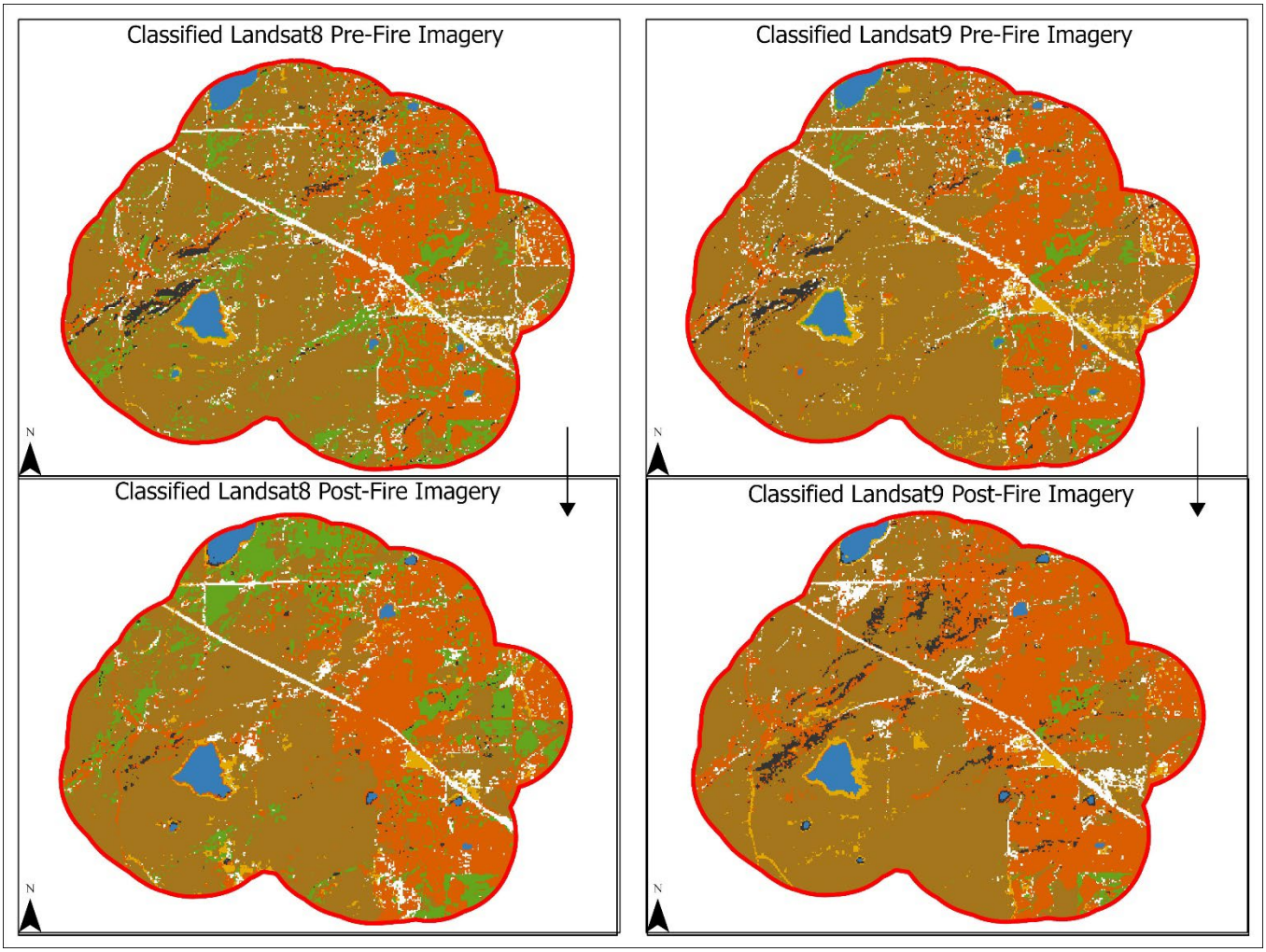

Figure 23. Comparison of pre- and post-fire image classification results.

With the images classified, the next step was to determine the amount of burned area within the Marshall Fire perimeter. Using the *Raster Calculator*, the Landsat8 Post-Fire imagery was subtracted from the Landsat8 Pre-Fire imagery to create a new raster image of the difference between the two. This process was also performed with the Landsat9 images to

create a difference raster. To create a binary image of burned and not-burned areas, the interim difference rasters were reclassified using the *Reclassify* tool to reassign pixels with a value of -1 (burned areas) to 1 and all other pixels reassigned to 0.

With the images classified and reclassified, the next step was to calculate the burned area from each image. First, the raster data needed to be converted to polygons using the *Raster to Polygon* tool; this created a multipart polygon based on pixel values (0 or 1). These new features were then clipped to the Marshall Fire perimeter to capture whether pixels were correctly classified within the known burn area. A new field, named "Acreage", was added to each of the features and calculated using the *Field Calculator* to convert the area value (square feet) to acreage.

4.4 Accuracy Assessment

To compare how accurately this process classified the different landcover and landuse classes, an accuracy assessment was performed on each of the pre- and post-fire images that resulted in four error matrix tables. The first step of the accuracy assessment was to use the *Create Accuracy Assessment Points* to create points to "ground truth" the classified results. 100 equally stratified random points were created and overlayed on each of the images. The equally stratified random sampling strategy was used as it creates an equal number of randomly distributed points across each of the classification classes. Each point's ground truth value was edited, if necessary, to match the landcover or landuse displayed in the image.

L9_preFire_AccuracyAssessmentPoints

Field: Add Calculate Selection: Select By

	OBJECTID *	SHAPE *	Classified	GrndTruth
1	1	Point	50	50
2	2	Point	10	10
3	3	Point	20	50
4	4	Point	10	10
5	5	Point	40	50
6	6	Point	30	30
7	7	Point	10	10
8	8	Point	10	10
9	9	Point	70	50
10	10	Point	40	20
11	11	Point	70	70
12	12	Point	20	20
13	13	Point	80	20

Figure 24. Example of the edited accuracy assessment points "ground truth" field.

Next, error matrices were created for each classified image and burn area rasters using the *Compute Confusion Matrix* tool with the "ground truthed" accuracy assessment points as an input.

4.5 Efficacy Test

Limitations in acquiring suitable satellite imagery (discussed below in Section 6.2) in the study's area of interest necessitated an efficacy test to objectively check the performance of the classification workflow described in this report. As this study was designed with a replicable workflow, the same steps were applied to a comparable study area in California.

The Thunder Fire burned just south of Bakersfield, California in Kern County between 06/22/2022 and 06/27/2022, burning close to 2,500 acres (CalFire, 2022). This study area

contains landcover and landuse classes found in the Marshall Fire study area, including barren, vegetation, grassland, and pavement. Water, shadow, and developed features were not present in the imagery. Landsat8 and Landsat9 imagery was also acquired from the USGS EarthExplorer, with one Landsat scene encompassing the project area. Each scene was projected to the California StatePlane Zone 5 projected coordinate system, which is used in Kern County, California. The Thunder Fire burn area perimeter was hand digitized using a georeferenced burn area image from the Cal Fire Active Fires of Interest web map, see appendix A, as no GIS data was available for this fire perimeter.

Figure 25. Results of the raster calculator operation to calculate the difference between the pre- and post-fire Landsat8 imagery and subsequent reclassification of pixel values to display a binary burn (pixel value 1) or unburned (pixel value 0) image. Red pixels represent burn areas while green represent unburned.

5. Results

5.1 Image Classification

The supervised pixel-based image analysis classification process successfully classified seven landcover and landuse features in the pre- and post-fire Landsat8 and Landsat9 images. Using these rasters, the acreage of each class was calculated and reported in Table 3 below.

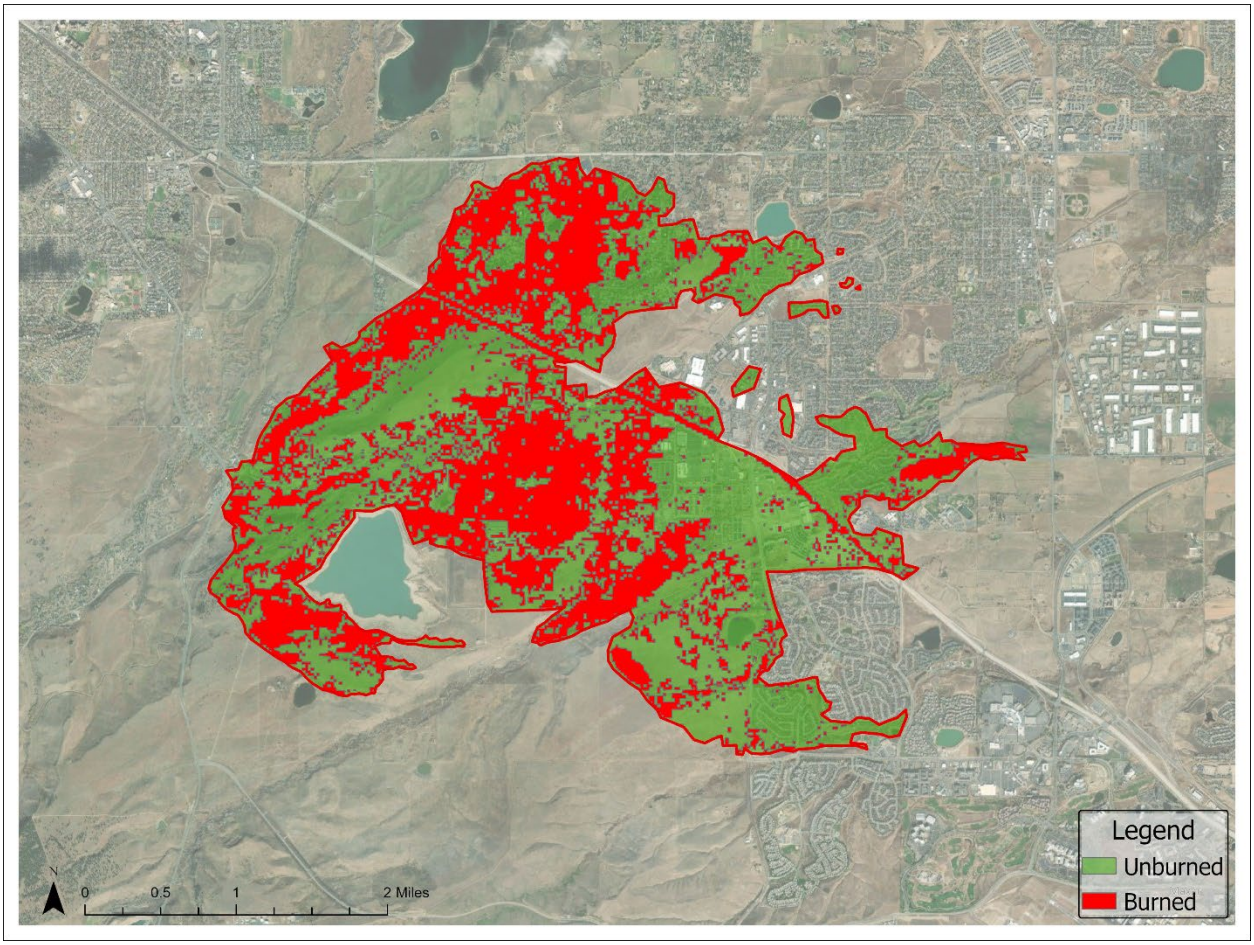

Figure 26. Results of the raster calculator operation to calculate the difference between the pre- and post-fire Landsat8 imagery and subsequent reclassification of pixel values to display a binary burn (pixel value 1) or unburned (pixel value 0) image. Red pixels represent burn areas while green represent unburned.

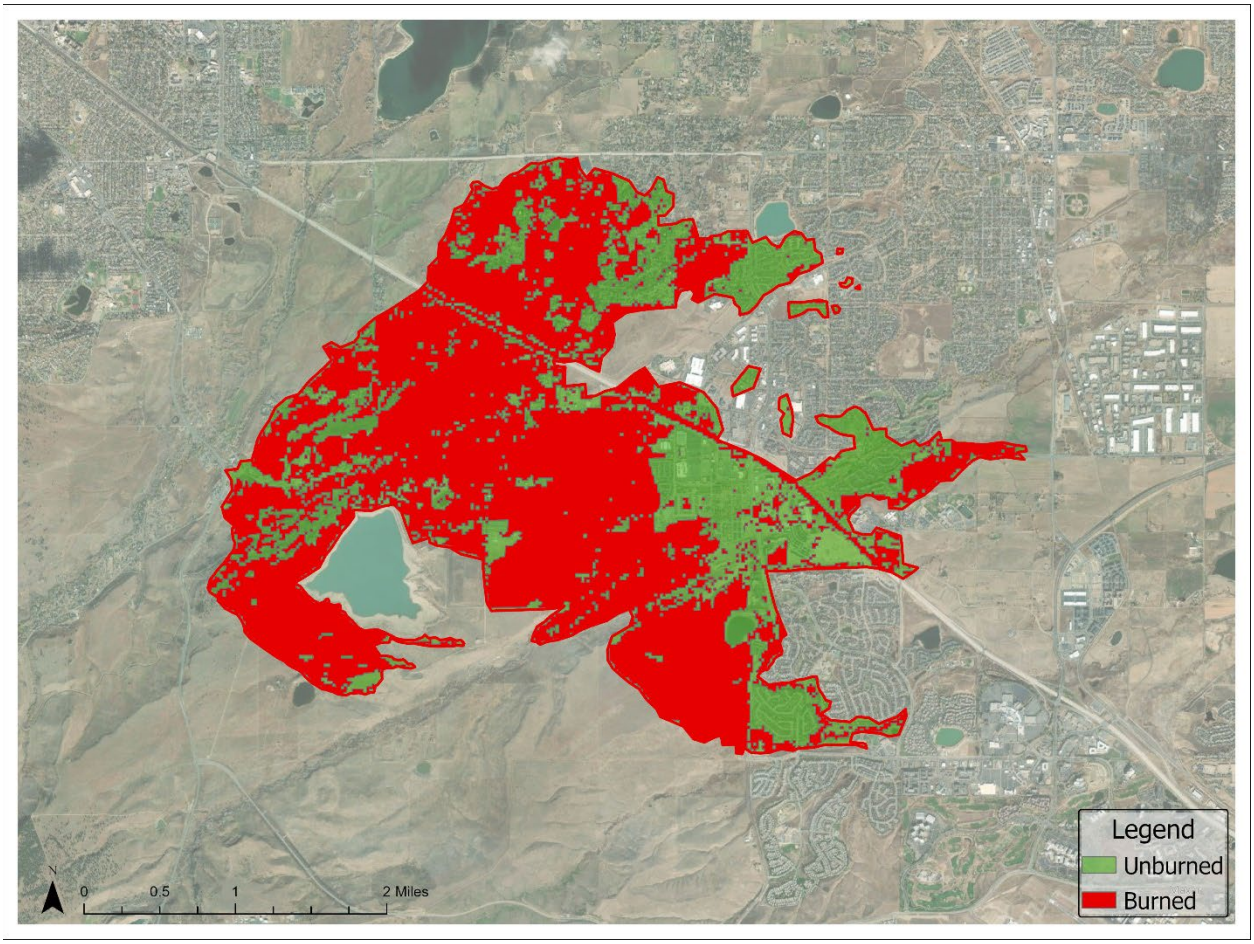

Figure 27. Results of the raster calculator operation to calculate the difference between the pre- and post-fire Landsat9 imagery and subsequent reclassification of pixel values to display a binary burn (pixel value 1) or unburned (pixel value 0) image. Red pixels represent burn areas while green represent unburned.

Image	Burned Area (acres)	Unburned Area (acres)
Landsat8	2,632.85	3,392.40
Landsat9	4,055.05	1,970.20

Table 3. Burned and unburned area totals.

5.2 Accuracy Assessment

The accuracy assessment reveals the classification process performed on the Landsat8 and Landsat9 images were not accurate enough to produce reliable results but does shed light

on the Landsat9 satellite's ability to better distinguish features based on their spectral signature.

5.2.1 Landsat8 Confusion Matrices

ClassValue	Water	Developed	Barren	Vegetation	Grassland	Pavement	Shadow	Total	User's Accuracy
Water	10	0	0	0	0	0	0	10	1
Developed	0	21	1	2	0	0	1	25	0.84
Barren	0	0	5	0	5	0	0	10	0.5
Vegetation	0	3	0	0	8	0	0	11	0
Grassland	0	2	0	0	50	0	0	52	0.96
Pavement	0	3	1	0	3	3	0	10	0.3
Shadow	0	0	0	0	1	0	9	10	0.9
Total	10	29	7	2	67	3	10	128	
Producer's Accuracy	1	0.72	0.71	0	0.75	1	0.9		0.77
									Overall Accuracy 0.68

Table 4. Error matrix created for Landsat8 pre-fire derived classified image.

Class	Water	Developed	Barren	Vegetation	Grassland	Pavement	Shadow	Total	User's Accuracy
Water	14	0	0	0	0	0	0	14	1
Developed	0	11	0	1	2	0	0	14	0.79
Barren	0	2	9	0	1	2	0	14	0.64
Vegetation	0	4	0	9	1	0	0	14	0.64
Grassland	0	0	1	0	13	0	0	14	0.93
Pavement	0	3	4	0	3	4	0	14	0.29
Shadow	0	3	0	0	1	0	10	14	0.71
Total	14	23	14	10	21	6	10	98	
Producer's Accuracy	1	0.48	0.64	0.9	0.62	0.67	1		0.71
									Overall Accuracy 0.67

Table 5. Error matrix created for Landsat8 post-fire derived classified image.

The error matrix displayed in Table 4 shows that of the 128 accuracy assessment points only 68% were correctly classified in their respective classes, and the overall accuracy of the error matrix in Table 5 is 1% less accurate. In each classification, water features were 100% accurately classified. Across the remaining classes, the classification process performed as expected: individual pixels in Landsat imagery can often contain multiple landcover or landuse classes, muddying the spectral characteristics of a pixel.

5.2.2 Landsat9 Confusion Matrices

Class	Water	Developed	Barren	Vegetation	Grassland	Pavement	Shadow	Total	User's Accuracy
Water	14	0	0	0	0	0	0	14	1
Developed	0	12	1	1	0	0	0	14	0.86
Barren	0	2	8	0	3	1	0	14	0.57
Vegetation	0	1	0	10	3	0	0	14	0.71
Grassland	0	0	0	0	14	0	0	14	1.00
Pavement	0	4	2	0	4	4	0	14	0.29
Shadow	0	1	0	0	0	0	13	14	0.93
Total	14	20	11	11	24	5	13	98	
Producer's Accuracy	1	0.60	0.73	0.91	0.58	0.80	1		0.77
									Overall Accuracy 0.73

Table 6. Error matrix created for Landsat9 pre-fire derived classified image.

Class	Water	Developed	Barren	Vegetation	Grassland	Pavement	Shadow	Total	User's Accuracy
Water	14	0	0	0	0	0	0	14	1
Developed	0	10	0	0	1	3	0	14	0.71
Barren	1	1	8	0	2	2	0	14	0.57
Vegetation	0	1	0	13	0	0	0	14	0.93
Grassland	0	1	0	0	13	0	0	14	0.93
Pavement	0	4	0	0	3	7	0	14	0.50
Shadow	1	2	0	0	0	0	11	14	0.79
Total	16	19	8	13	19	12	11	98	
Producer's Accuracy	0.875	0.53	1.00	1.00	0.68	0.58	1		0.78
									Overall Accuracy 0.74

Table 7. Error matrix created for Landsat9 post-fire derived classified image.

The error matrix displayed in Table 6 shows that of the 98 accuracy assessment points 73% were correctly classified in their respective classes, and the overall accuracy of the error matrix in Table 7 is 1% more accurate. In each classification, shadow features were 100% accurately classified, while water features were incorrectly classified in the Landsat9 post-fire imagery twice (once as a barren feature and once as a shadow feature) for a producer's accuracy of 87.5%. Barren and vegetation classification's accuracy were high in the pre-fire classification and increased to 100% accurately classified in the post-fire imagery. Pavement and developed classification decreased in accuracy in the post-fire imagery.

5.3 Results of Efficacy Test

The image classification process replicated for the efficacy test successfully classified the landcover and landuse features in the Thunder Fire study area. Performing the classification on the Landsat8 and Landsat9 imagery resulted in the following burn area calculations:

Image	Burned Area (acres)	Unburned Area (acres)
Landsat8	2289.39	170.92
Landsat9	1974.74	499.77

Table 8. Burned and unburned acreage extracted from the Thunder Fire classified imagery.

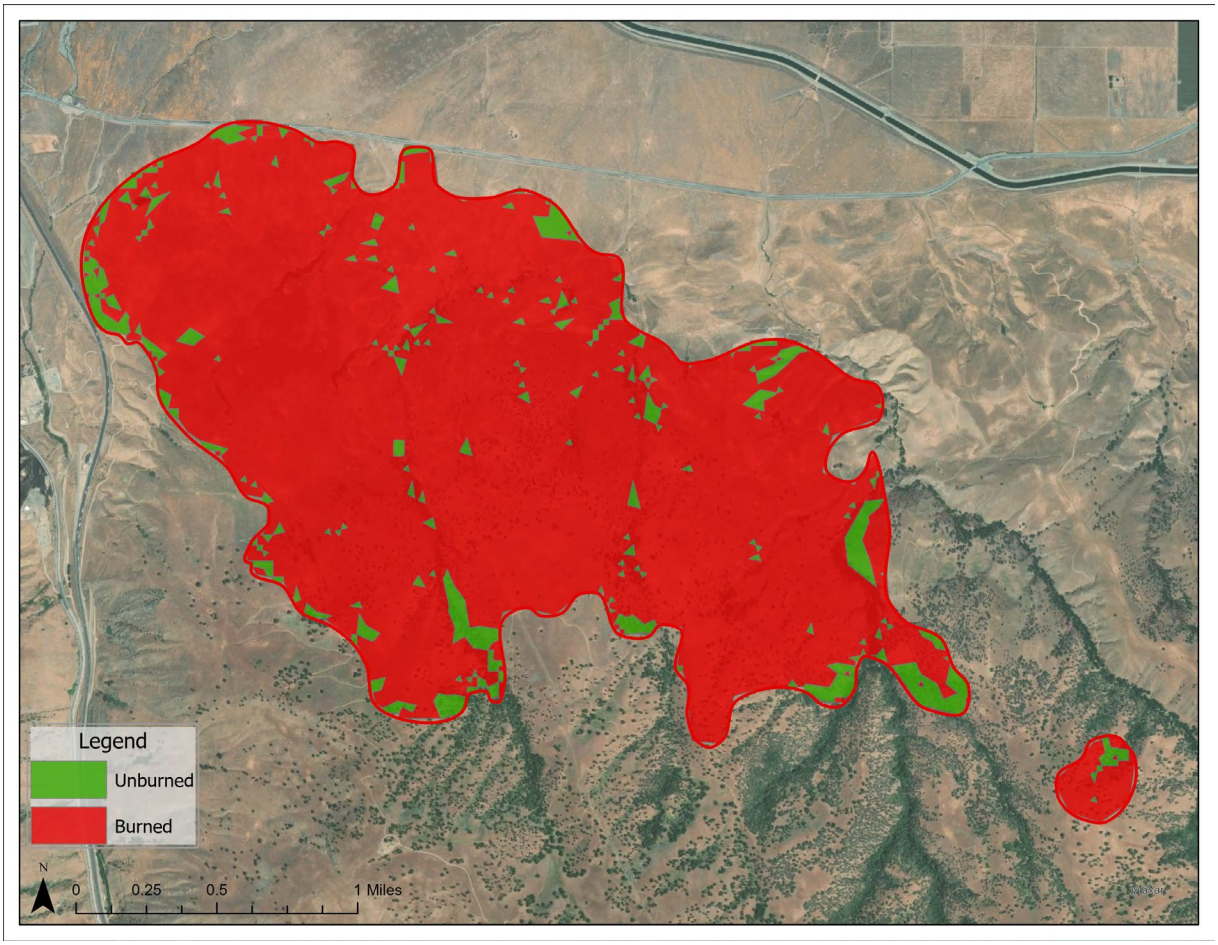

Figure 28. Results of the raster calculator operation to calculate the difference between the pre- and post-fire Landsat8 imagery and subsequent reclassification of pixel values to display a binary burn (pixel value 1) or unburned (pixel value 0) image of the Thunder Fire study area. Red pixels represent burn areas while green represent unburned.

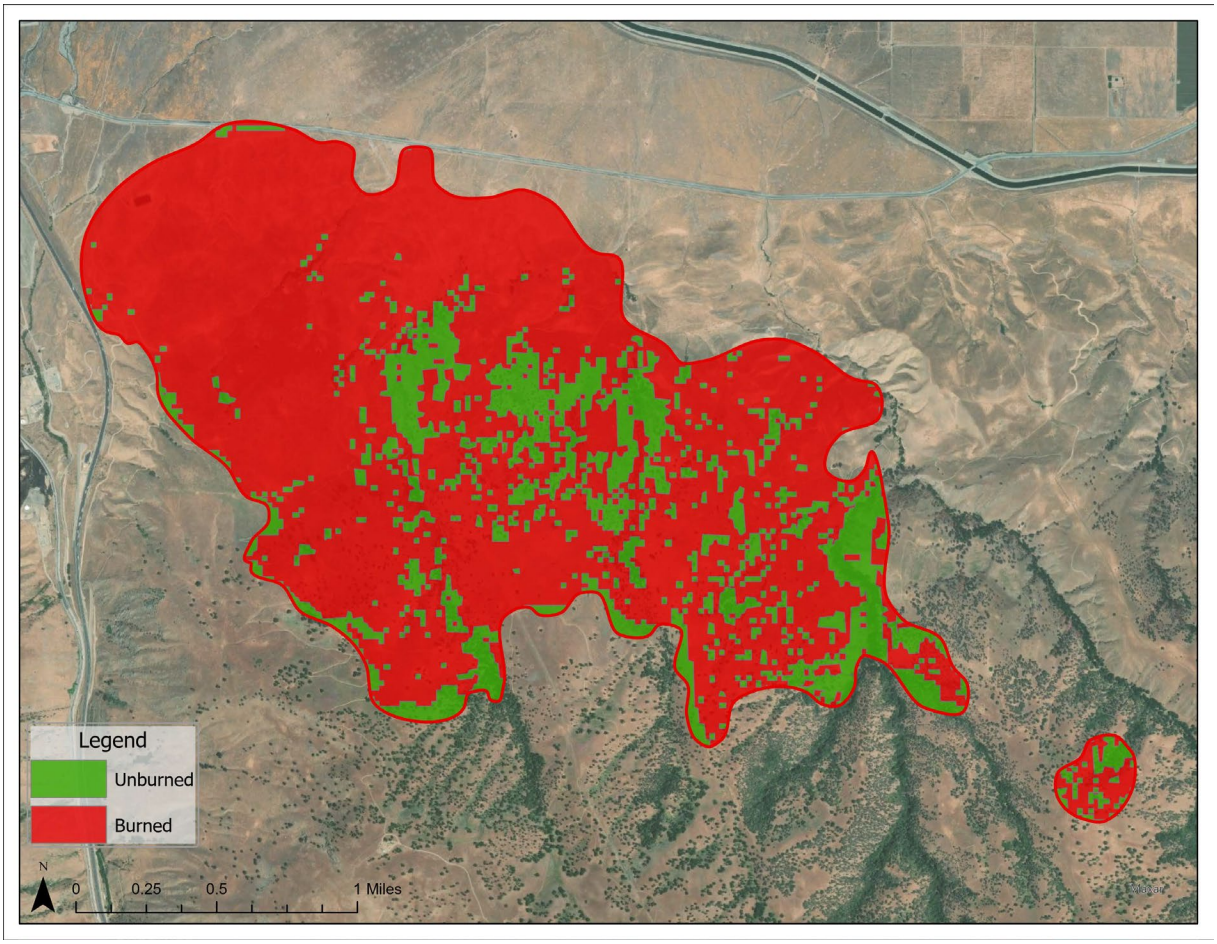

Figure 29. Results of the raster calculator operation to calculate the difference between the pre- and post-fire Landsat9 imagery and subsequent reclassification of pixel values to display a binary burn (pixel value 1) or unburned (pixel value 0) image of the Thunder Fire study area. Red pixels represent burn areas while green represent unburned.

5.3.1 Landsat8 Confusion Matrices (Thunder Fire)

Class	Barren	Vegetation	Grassland	Pavement	Total	User's Accuracy
Barren	6	0	3	0	9	0.7
Vegetation	0	10	7	0	17	0.59
Grassland	3	3	67	0	73	0.92
Pavement	0	0	0	1	1	1
Total	9	13	77	1	100	
Producer's Accuracy	0.67	0.77	0.87	1		0.84
					Overall Accuracy	0.61

Table 9. Error matrix created for Landsat8 Thunder Fire pre-fire derived classified image.

Class	Barren	Vegetation	Grassland	Pavement	Total	User's Accuracy
Barren	72	4	9	0	85	0.8
Vegetation	4	4	2	0	10	0.40
Grassland	3	1	8	0	12	0.67
Pavement	1	0	0	9	10	0.9
Total	80	9	19	9	117	
Producer's Accuracy	0.9	0.44	0.42	1		0.79
					Overall Accuracy	0.57

Table 10. Error matrix created for Landsat8 Thunder Fire post-fire derived classified image.

The error matrix in Table 9 shows that of the 100 accuracy assessment points 61% were correctly classified in their respective classes, showing the Barren landcover class was the least accurately classified. Overall, the Landsat8 pre-fire classification was 61% accurate. In table 10, the overall accuracy of the Landsat8 post-fire classification was 57%. Grassland and vegetation classes were the least accurately classified, with 44% and 42% accuracy. In each classification, pavement features were 100% accurately classified.

5.3.2 Landsat9 Confusion Matrices (Thunder Fire)

Class	Barren	Vegetation	Grassland	Pavement	Total	User's Accuracy
Barren	14	1	1	0	16	0.9
Vegetation	0	25	1	0	26	0.96
Grassland	0	0	33	0	33	1
Pavement	0	0	7	18	25	0.72
Total	14	26	42	18	100	
Producer's Accuracy	1	0.96	0.79	1		0.9
					Overall Accuracy	0.86

Table 11. Error matrix created for Landsat9 Thunder Fire pre-fire derived classified image.

Class	Barren	Vegetation	Grassland	Pavement	Total	User's Accuracy
Barren	25	0	0	0	25	1.0
Vegetation	1	24	0	0	25	0.96
Grassland	1	0	24	0	25	0.96
Pavement	0	0	6	19	25	0.76
Total	27	24	30	19	100	
Producer's Accuracy	0.93	1.00	0.80	1		0.92
					Overall Accuracy	0.89

Table 12. Error matrix created for Landsat9 Thunder Fire post-fire derived classified image.

The error matrix displayed in Table 11 shows that 86% of classes were correctly classified and the overall accuracy of the error matrix in Table 12 is 3% more accurate, for an overall accuracy of 89%. In each classification, each class's accuracy was high with the lowest performing class being Grassland. Each Pavement feature was correctly classified in both the pre- and post-fire image. The remaining classes wavered between a couple percentage points, some gaining accuracy in the post-image classification.

6. Synthesis and Conclusions

6.1 Synthesis

The classification process performed on the pre- and post-fire imagery captured by Landsat8 and Landsat9 satellites successfully classified burned and non-burned areas within the Marshall Fire perimeter. While the results of the classification were not reliably accurate, the workflow presented is replicable and can be adjusted to produce better results. Although the low accuracy of the process signals a need to revisit the training samples created, creating a new set of training samples may not increase the accuracy very much due the spatial resolution

of Landsat satellite imagery. Landsat has a 30-meter spatial resolution which means each pixel represents 30 meters on the ground, leading to the potential to contain mixed landuse or landcover in a single pixel. Pixel samples with mixed spectral characteristics lead to a variety of spectral signatures and poor classifications.

Overall, the accuracy assessment shows that the Landsat9 imagery produced 5% more accurate results than the Landsat8 imagery. These results are modest as greater gains in accuracy were expected with Landast9's improved radiometric resolution. The accuracies reported in Tables 4 thru 7 are within the range of accuracies reported in similar studies using Landsat8 imagery. Tassi et al (2021) reported an overall accuracy of about 81%, with individual classes falling between 76% and almost 85% accuracy. Other studies report higher accuracies: Roy et al (2019) reported an overall accuracy of 92% mapping burned areas in Southern Africa and Elhag et al (2020) reported an overall accuracy of 69% mapping burned areas in Greece. The Landsat9 pre-fire imagery more accurately classified barren, vegetation, and shadow features and in the post-fire imagery, the Landsat9 greatly increased in the accuracy of classification of the developed, barren, vegetation, and grassland classes. Using these classified images to create a burn area raster of the Marshall Fire resulted in accurately identifying 4,055.05 acres of burned area within the known fire perimeter.

Finally, the reported acreage of the final burn area of the Marshall Fire is 6,025 acres (Camero, 2021), and it appears this value does not exclude pockets of unburned areas within the fire perimeter. Combining the burned and unburned areas for each image equates to roughly 6,025 acres.

6.2 Limitations & Next Steps

Limitations affecting this analysis include the inability to visit the area of interest to truly ground truth the image classification, limited access to eCognition software to develop comprehensive spectral interpretation keys, and snow present in imagery after the fire was contained.

In remote sensing, the term "ground truth" refers to collecting information on location. The process of ground truthing allows for creating information related to real features and materials on the ground in a project's area of interest, improving the interpretation of classified images. Instead of traveling to visit the Marshall Fire burn area in Colorado, I edited the accuracy assessment "ground truth" points by referencing the Landsat images for each time period.

eCognition is "…an advanced analysis software for geospatial applications," (Trimble, n.d.) often used to interpret features in raster datasets. Different classification workflows, like object-based image classification, involve image segmentation to "cut" an image into pieces based on attributes like shape, color, and feature's positions relative to another. While this analysis did not involve object-based workflows, using eCognition's image segmentation tools could have helped to create image interpretation keys to reference when evaluating whether the spectral profile charts created from the training samples for each class were adequate for the image classifier. While the spectral profiles created provided enough information to continue the analysis, not having comprehensive interpretation keys could have negatively affected the results.

Finally, burn scar detection and burn area mapping is usually completed during a fire and immediately following containment to ensure accurate perimeters are drawn and used as reference. The 2021/2022 Marshall Fire was extinguished overnight due to eight inches of snowfall (Sullivan, 2022). While this weather event was certainly welcomed to naturally contain the fire, it limited the ability to find snow-free imagery immediately following the fire's containment. Snow free post-fire imagery captured by the Landsat8 and Landsat9 satellites was not available until April, three months after the Marshall Fire was contained. Snow melt due to above-average spring temperatures fueled vegetation growth, obscuring the burn scar and introducing landcover classes into the burn area that could have affected the classification process and explain the modest improvement in accuracy of the Landsat9 classified images.

To address the limitation of unsuitable post-fire imagery, an efficacy test of this image classification process was conducted. Performing this workflow on an additional set of imagery for the June Thunder Fire in Southern California resulted in higher and improved accuracy, as were the predicted results of this project. The Landsat9 pre-fire classified imagery marked a 25% increase in overall accuracy when compared to the Landsat8 classification (86% compared to 61%) and the post-fire classified imagery was 32% more accurate (89% compared to 57%). The unobscured imagery allowed for better comparison of the accuracies of the image classification to evaluate the improvement of the radiometric resolution of the Landsat9 satellite over Landsat8. While the increase in overall accuracy was expected, the increase seen in classifying the Thunder Fire burn area could be attributed to decrease in the number of classes. Thinh et al (2019) performed a literature review of over 100 papers, "…to examine the relationship between overall accuracy and the number of classification classes…" and found

negative correlation between the overall accuracy and number of classes where an addition of a single class lead to a decrease of 77% overall accuracy. Conversely, reducing the number of classes can lead to an increase in overall accuracy. In their review, Thinh et al (2019) found that in 64 studies the highest accuracy of 98.7% was achieved with only 4 classes while the lowest accuracy of 42% with 29 classes.

6.3 Conclusions

As the number and severity of wildfires increase across the United States, our fire and emergency response agencies need reliable and accurate data products to assist in their responding to and managing these disaster events. Remote sensing technologies have been adopted for use in fire mapping, including burn scar detection utilizing burn indices and burn area mapping utilizing image classification schemes to detect changes in an environment where a fire has occurred. The developments made by the National Land Imaging Program to the Landsat missions marks an important evolution in remote sensing technology. The ability to distinguish over 16,00 shades in a single wavelength will only increase our capacity to more accurately detect and map wildfires and their effects, as demonstrated in this paper. The results of the Marshall Fire image classification were reinforced by performing an additional image classification of the Thunder Fire burn area, which resulted in accuracy gains between 25% and 32%. By using remotely sensed images from the Landsat9 satellite GIS and remote sensing professionals can provide more accurate and reliable products to wildfire preparation, detection, response, and mitigation agencies.

Sources

Andone, D., & Maxouris, C. (2021, December 31). *No deaths have been reported in the ferocious Colorado wildfire. it may be a 'New Year's miracle,' governor says*. CNN. Retrieved July 10, 2022, from https://www.cnn.com/2021/12/31/us/colorado-wildfires-friday/index.html

Bellisle, M. (2022, January 2). *Climate change, new construction mean more ruinous fires*. AP NEWS. Retrieved July 10, 2022, from https://apnews.com/article/climate-wildfires-science-environment-environment-and-nature-8d111d6f6dfa9bfa78a2fe9659802826

Boulder County GIS. (2022). GIS FAQ. Retrieved February 24, 2022, from https://www.bouldercounty.org/property-and-land/geographic-information-systems/frequently-asked-questions/#1491412190974-a119b475-c373

Colorado State Plane, North Zone projection, based upon the 1992 HARN adjustment of the 1983 North American Datum (NAD HPGN 83/92).

Camero, K. (2021, December 31). *Most destructive wildfire in Colorado's history wreaked havoc. Here's what to know*. The Sacramento Bee. Retrieved July 10, 2022, from https://www.sacbee.com/news/nation-world/national/article256962277.html

California Department of Forestry and Fire Protection (CAL FIRE). (n.d.). *Incidents overview*. Cal Fire Department of Forestry and Fire Protection. Retrieved July 31, 2022, from https://www.fire.ca.gov/incidents/

California Department of Forestry and Fire Protection (CAL FIRE). (2022, June 27). *Thunder fire incident*. Cal Fire Department of Forestry and Fire Protection. Retrieved July 31, 2022, from https://www.fire.ca.gov/incidents/2022/6/22/thunder-fire/

Elhag, M., Yimaz, N., Bahrawi, J., & Boteva, S. (2020). Evaluation of optical remote sensing data in burned areas mapping of Thasos Island, Greece. *Earth Systems and Environment*, *4*(4), 813–826. https://doi.org/10.1007/s41748-020-00195-1

Esri. (n.d.). *Spectral profile*. Spectral profile-ArcGIS Pro | Documentation. Retrieved July 11, 2022, from https://pro.arcgis.com/en/pro-app/2.8/help/data/imagery/spectral-profile-chart.htm

NASA Landsat Science. (n.d.). Building on the Landsat Legacy [Timeline of the Landsat program]. Retrieved March 04, 2022, from https://landsat.gsfc.nasa.gov/satellites/landsat-9/

Pereira, J. M., Sá, A. C., Sousa, A. M., Silva, J. M., Santos, T. N., & Carreiras, J. M. (1999). 7. Spectral characterization and discrimination of burnt areas. In *Remote Sensing of Large*

Wildfires (pp. 123-138). New York: Springer, Berlin, Heidelberg. doi:https://doi.org/10.1007/978-3-642-60164-4_7

USGS. (n.d.-a). Landsat 8. Retrieved March 4, 2022, from https://www.usgs.gov/landsat-missions/landsat-8

USGS. (n.d.-b). Landsat 9. Retrieved March 4, 2022, from https://www.usgs.gov/landsat-missions/landsat-9

OpenData Boulder County. (2022). Marshall Fire perimeter. Boulder County, Colorado; Boulder County, Colorado.

https://opendata-bouldercounty.hub.arcgis.com/datasets/bouldercounty::wildfire-history/explore?location=39.927093%2C-105.145175%2C14.88

Roy, D. P., Huang, H., Boschetti, L., Giglio, L., Yan, L., Zhang, H. H., & Li, Z. (2019). Landsat-8 and sentinel-2 burned area mapping - a combined sensor multi-temporal change detection approach. *Remote Sensing of Environment*, *231*. https://doi.org/10.1016/j.rse.2019.111254

Sparig, J. (2022). *Marshall Fire consumes residence in Boulder County, Colorado*. TheColoradoSun. Retrieved July 7, 2022, from https://coloradosun.com/2022/01/30/marshall-fire-underground-coal-fire/.

Sullivan, B. (2022, January 1). *Snow puts out Colorado wildfires with 3 people missing and nearly 1,000 homes burned*. NPR. Retrieved July 20, 2022, from https://www.npr.org/2022/01/01/1069639530/colorado-wildfire-missing

Tassi, A., Gigante, D., Modica, G., Di Martino, L., & Vizzari, M. (2021). Pixel- vs. object-based Landsat 8 data classification in Google Earth engine using Random Forest: The case study of maiella national park. Remote Sensing, 13(12). https://doi.org/10.3390/rs13122299

Thinh, T. V., Duong, P. C., Nasahara, K. N., & Tadono, T. (2019). How does land use/land cover map's accuracy depend on number of classification classes? SOLA, 15, 28–31. https://doi.org/10.2151/sola.2019-006

Trimble. (n.d.). *What is ecognition?* Trimble Geospatial. Retrieved July 20, 2022, from https://geospatial.trimble.com/what-is-ecognition

Van Denburg, H. (2022). *Wildfire flames and smoke rise above Superior, Colorado, on Thursday, Dec. 30, 2021*. CPR News. Retrieved July 7, 2022, from https://www.cpr.org/2022/01/05/boulder-county-marshall-fire-timeline/.

Woo, H., Acuna, M., Madurapperuma, B., Jung, G., Woo, C., & Park, J. (2021). Application of maximum likelihood and spectral angle mapping classification techniques to evaluate forest fire severity from UAV multi-spectral images in South Korea. *Sensors and Materials*, *33*(11). https://doi.org/10.18494/sam.2021.3365